Journal of Hydrology: Regional Studies 42 (2022) 101127

Contents lists available at ScienceDirect

Journal of Hydrology: Regional Studies

journal homepage: www.elsevier.com/locate/ejrh

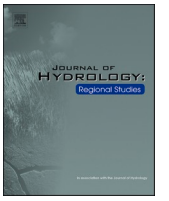

A hydro-economic analysis of end-of-century climate projections on agricultural land and water use, production, and revenues in the U.S. Northern Rockies and Great Plains

Zachary H. Lauffenburger [a,*], Marco P. Maneta [a,c], Kelly M. Cobourn [b], Kelsey Jencso [c], Brian Chaffin [c], Anna Crockett [c], Bruce Maxwell [d], John S. Kimball [c]

[a] Department of Geosciences, University of Montana, Missoula, MT, USA
[b] Department of Forest Resources and Environmental Conservation, Virginia Tech, Blacksburg, VA, USA
[c] W.A. Franke College of Forestry & Conservation, University of Montana, Missoula, MT, USA
[d] Land Resources and Environmental Sciences, Montana State University, Bozeman, MT, USA

ARTICLE INFO

Keywords:
Water management
Irrigated agriculture
Rainfed agriculture
Climate variability
-Economic variability
Remote Sensing

ABSTRACT

Study region,Montana, U.S.A. Study focus Creating adaptation plans for projected imbalances in the western U.S. agricultural water demand-supply system are difficult given uncertainty in climate projections. It is critical to understand the uncertainties and vulnerabilities of the regional agricultural system and hydrologic impacts of climate change adaptation. We applied a stochastic, integrated hydro-economic model that simulates land and water allocations to analyse Montana farmer adaptations to a range of projected climate conditions and the response of the hydrologic system to those adaptations. Satellite observations of crop types, productivity, water use, and land allocation were used for model calibration. A suite of climate models was employed to quantify end-of-century impacts on streamflows, water and land use, production, and net revenues.New hydrological insights for the region Simulations showed summer streamflows were influenced by a state-wide 18.2% increase in agricultural water use. Decreased summer water availability with increased demand could have far reaching impacts downstream. Land use for irrigated crops increased 1.6%, while rainfed crops decreased 6.5%, implying state-level decrease in planted area. Even with increased land and water use for irrigated crops, production decreased 0.5%, while rainfed production decreased 2.7%. Corresponding losses in net revenues totaled 1.5% and 7.2% for irrigated and rainfed crops, respectively.Results highlight vulnerabilities of semi-arid agricultural regions and can aid water managers in sustaining agriculture in these regions.

1. Introduction

Agriculture in the western United States (U.S.) is critical to the nation's cattle, barley, and wheat production. Production of these commodities in the arid and semi-arid West is highly dependent on seasonal precipitation and irrigation. Ongoing climate change

* Corresponding author.
E-mail addresses: zachary1.lauffenburger@umontana.edu (Z.H. Lauffenburger), marco.maneta@mso.umt.edu (M.P. Maneta), kellyc13@vt.edu (K.M. Cobourn), kelsey.jencso@umontana.edu (K. Jencso), brian.chaffin@umontana.edu (B. Chaffin), anna.crockett@umconnect.umt.edu (A. Crockett), bmax@montana.edu (B. Maxwell), john.kimball@umontana.edu (J.S. Kimball).

https://doi.org/10.1016/j.ejrh.2022.101127
Received 1 February 2022; Received in revised form 18 May 2022; Accepted 30 May 2022
Available online 8 June 2022

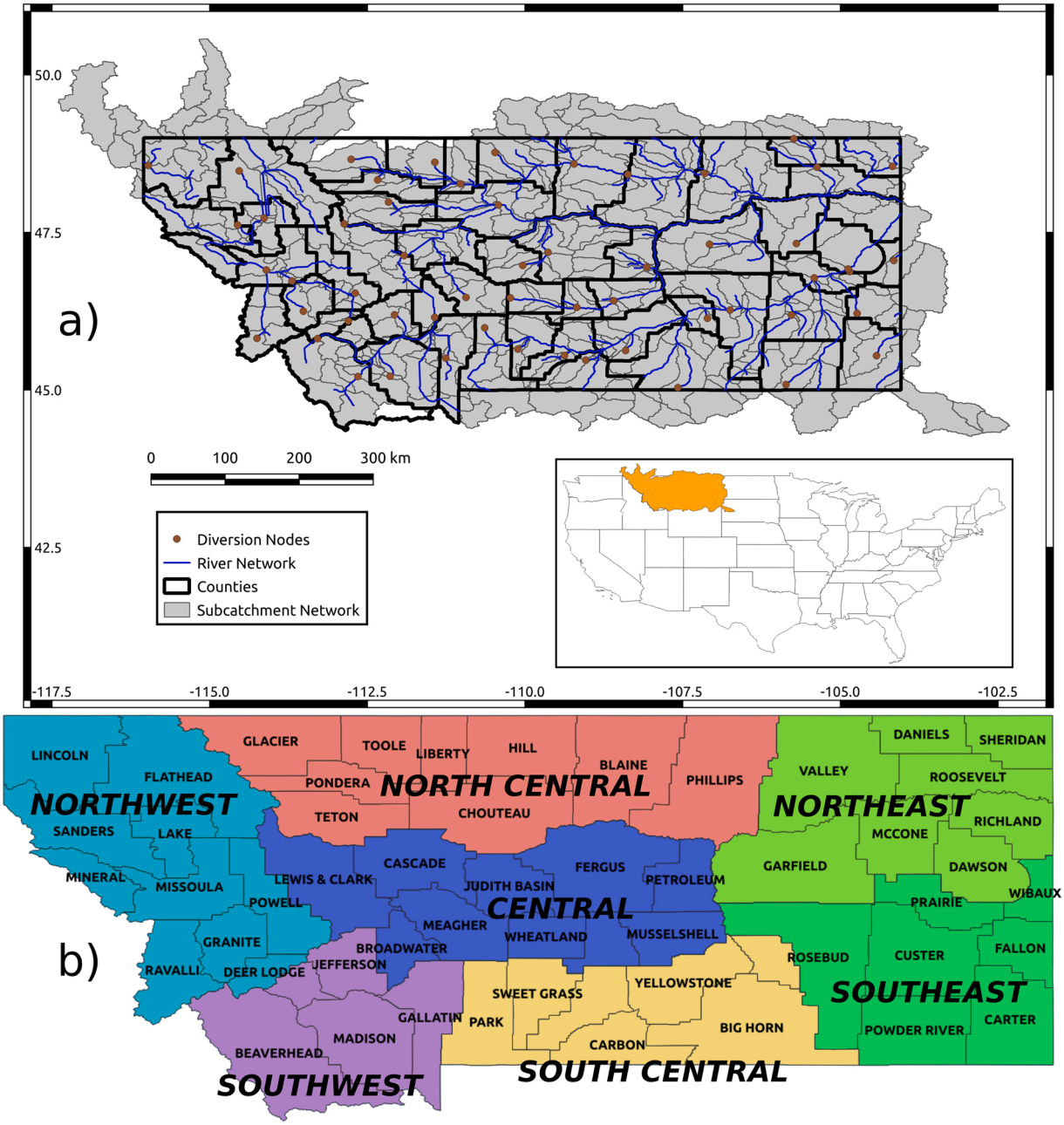

Fig. 1. a) Location of the study region and representation of the elementary sub-catchment network (grey polygons), river network (blue polylines), water diversion nodes (brown points), and Montana county outlines (black polygons). b) Montana's counties and climate regions.

coupled with growing water demands is placing the region's water system under increased pressure. In many cases the water demands already exceed average supplies (Anderson et al., 2018; Averyt et al., 2013; Ficklin et al., 2013; Grantham and Viers, 2014; Slaughter et al., 2010; Ward et al., 2006). Throughout the West, farmers respond to temporal variations in climate, water availability, and market and policy signals by changing water allocations, crops grown, and land apportionment to each of the crops. Irrigation in the western U.S. has generally increased over the last century, but at varying paces across different agricultural regions (Edwards & Smith, 2018). In arid and semi-arid regions, irrigation water availability allows farmers to reduce exposure to periods of precipitation shortfall and to meet increasing demands for agricultural products (Hanjra et al., 2009; Schaible et al., 2010; Tack et al., 2017; Warrick and Gardner, 1983); however, potential climate change impact on water supplies is increasing the risk for farmers. With current water sources committed and fewer opportunities to develop new sources, irrigators and water managers will need to become more efficient with existing water supplies.

Hydro-economic models have been utilized by water resource managers for decades (Brouwer and Hofkes, 2008; Harou et al., 2009). These models are used at various spatial and temporal scales to analyze, anticipate and manage competing demands between water supply systems and agriculture under different climate extremes (Esteve et al., 2015; Falloon and Betts, 2010; Maneta et al., 2009; Medellín-Azuara et al., 2011; Torres et al., 2012; Ward et al., 2006), and the influence of economic and policy scenarios (Ghosh et al., 2014; Howitt et al., 2012; Varela-Ortega et al., 1998). There are numerous studies that implement hydro-economic models with a focus on irrigated agriculture (Borrego-Marín et al., (2020); Connell-Buck et al., 2011; Ghosh et al., 2014; Medellín-Azuara et al., 2011; Ward et al., 2006), but fewer studies have focused on regions with mixed rainfed and irrigated crops (Maneta et al., 2009; Siderius et al., 2016). Conversion of rainfed to irrigated cropland will increase pressure on water resources as climate change progresses (Lauffenburger et al., 2018). In the past it was difficult to accurately quantify land use (LU) allocated to rainfed and irrigated crops but advances in remote sensing technology have helped fill this data gap (Colligan et al., 2021; Ketchum et al., 2020).

In this study we analyze producer adaptive behavior in the state of Montana using a regional scale hydro-economic model forced with end-of-century climate projections from a suite of downscaled climate models. Farming and ranching activity in the state of Montana is representative of the larger U.S. Northern Rocky Mountains region. The hydro-economic model was recently developed and calibrated for regional-scale analysis and incorporates observational and climate projection uncertainty in its predictions. A novelty is that the model calibration leverages a decade-long remote sensing record of agricultural activity (cropland allocation, production and crop evapotranspiration) and advances in remote sensing data assimilation methods. We use model results to analyze the potential impacts of projected climates on streamflow (SF), water diversions (WD), agricultural LU and water use (WU), and crop production (PD) and farm net revenues (NR) in Montana, a state that includes portions of both the Northern Rockies and Northern Great Plains (NGP). A key objective of this study is to quantify the net hydro-economic impact attribu` to producer adaptive response to projected worse-case end-of-century conditions as represented by the Representative Concentration Pathway (RCP) 8.5 scenario. We isolated the net effects of farmer adaptive decision-making, by assuming policy and technology status-quo, i.e., no development of new water sources, no irrigation infrastructure adaptations, no new crop types or varieties, and no policy changes to water rights or access to water resources. The results reflect the end-member impact scenario for producers if no action is taken.

This study overcomes some limitations of previous studies by calibrating the model with observations from an extended spatial and temporal period that covers a wide range of climatic and economic conditions, and by explicitly treating the effect of observation and climate projection uncertainty in the results. The specific objectives of this study are (1) to reveal the impacts of climate change in rural regions of the agricultural western U.S.; (2) to determine the crop types that farmers are more likely to prioritize under future climates; and (3) to investigate the economic and hydrologic costs of farmers' adaptive measures to climate change. Our study provides insight on the specific topic of agricultural vulnerability to climate that water resource managers can consider to inform effective agricultural water policy.

2. Study region

Situated in the Northern Rocky Mountain range and straddling the continental divide, Montana (Fig. 1a) includes part of the Intermountain West and the NGP. The northwest and southwest regions (Fig. 1b) are characterized by mountains, valleys, milder winters, cooler summers, and more year-round precipitation, while the central and eastern regions are characterized by warmer summers, colder winters, and less precipitation (Silverman et al., 2017). The topographic and climatic gradients across Montana have a strong influence on SF and LU. The western watersheds tend to be smaller, but considerably wetter than the eastern watersheds, resulting in most of the state's surface water flowing into the Columbia River basin (MT DNRC, 2014). The topography of the western watersheds is a factor in the distribution of land properties that favors smaller farms and ranches located in the mountain valleys. The central and eastern watersheds are considerably larger and the agricultural land holdings more extensive, but surface water is less accessible except along the main river corridors. While dryland and irrigated agriculture are practiced across the state most of the irrigated acreage occurs in western Montana while eastern Montana is primarily rainfed (MT DNRC, 2014; USDA NASS, 2017). Roughly 96% of total water withdrawals are used for irrigated agriculture, and 98% of those withdrawals come from surface waters (U. S. Geological Survey (USGS), 2018).

Agriculture is a major contributor to Montana's gross domestic product and critical in supporting rural livelihoods. According to the 2017 Census of Agriculture, alfalfa, barley, spring wheat, and winter wheat dominate Montana's agriculture both in NR and LU; these four crops collectively accounted for over $2 billion in revenues and over 54% of the total cropland area (USDA NASS, 2017). Alfalfa PD, mainly to support the cattle industry, is ubiquitous state-wide, with the central and southwest regions (Fig. 1b) being the most productive. The north central region was dominated by barley PD. Roughly 27% of all LU to irrigated barley was in Teton County. Approximately 76% of all spring wheat PD occurred in the north central and northeast regions, much of which was non-irrigated. While winter wheat was produced across the state, a cluster of 11 counties in the north central and central regions, known as the "Golden Triangle", accounted for approximately 81% of the state's total PD, with Chouteau County alone accounting for 24%. Although irrigation of winter wheat occurred in 11 counties in the eastern half of the state, the acreage values were low and therefore our study assumes all winter wheat is rainfed.

3. Methods

3.1. Hydro-economic model

In our analysis we applied a stochastic hydro-economic modeling framework that integrates climate, surface and subsurface

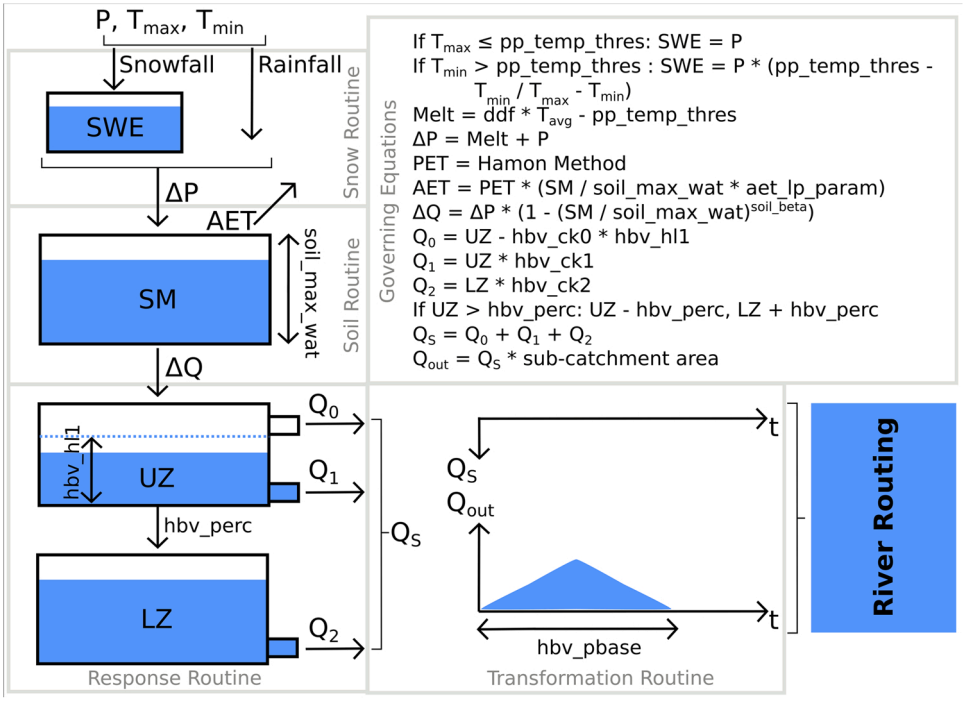

Fig. A1. Conceptual structure of the modified HBV model (model inputs and outputs and model state variables in capital letters; model parameters in lower case letters).

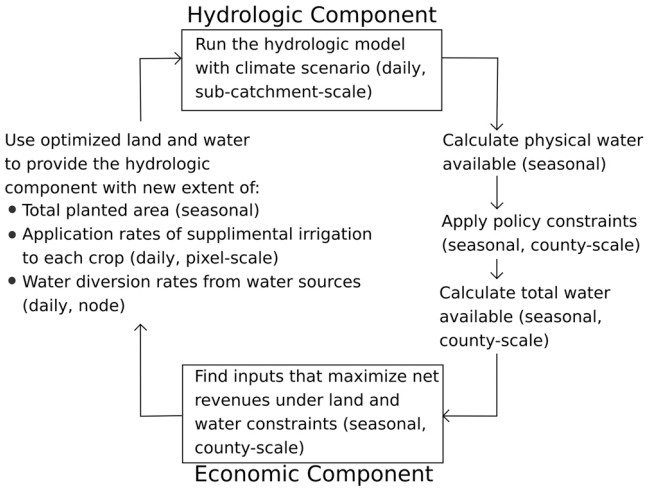

Fig. 2. Schematic of the interactions and feedbacks between the hydrologic and the economic components of the model. The components iterate until the economic model converges to a state that is consistent with the available land and water resources.

hydrology, agronomy, economics of agricultural production and institutional constraints (Maneta et al. 2020). A comprehensive description of the model and the calibration method is provided in Appendices A, B, and C, but here we present an overview of the structure and processes simulated relevant to interpret the results. Our hydro-economic model integrates a semi-distributed hydrologic model that simulates the rainfall-runoff and water routing processes through the hydrologic network of the study region (Fig. 1a). We implemented a gridded version of the Hydrologiska Byråns Vattenbalansavdelning (HBV) model (Bergström and Forsman, 1973; Bergström, 1995; Lindström et al., 1997) to simulate daily sub-catchment runoff (Fig. A1) in combination with the Muskingum-Cunge model (Cunge,1969) to route daily streamflows through the river network. The agroeconomic component of the model simulates agricultural water demands, which are used to calculate WD at specific river nodes (Fig. 1a). The river network propagates the effects of agricultural WD downstream in the form of reduced SF available to downstream users.

The agroeconomic component of the model relies on the assumption that farmers have historically allocated resources (land and

Table 1
Hydro-economic model inputs required for scenario simulations. Superscripts: D denotes the input is deterministic, S denotes the input is stochastic, VS denotes the input varies spatially, and CS denotes the input is constant spatially.

Input	Units	Source	Resolution
Precipitation^{D,VS}	mm	MACA (Abatzoglou, 2013)	4 km, daily
Temperature^{D,VS}	°C	MACA (Abatzoglou, 2013)	4 km, daily
Crop prices^{S,CS}	$	USDA NASS (2015)	State-level, annual
Production costs per crop per unit land^{S,CS}	$/ha	USDA NASS (2015)	State-level, annual
Cost of water^{S,CS}	$/mm-ha	USDA NASS (2015)	State-level, annual
Crop development stages^{D,CS}	day	USBR (2016) AgriMet	State-level, daily
Irrigation-system efficiency^{D,CS}	%	MT DNRC (2017)	County-level, annual
Crop water use baseline^{S,VS}	mm-ha	Remote sensing (He et al., 2019)	30 m, 8 day (aggregated to county-level, annual)
Crop water use end-of-century^{S,VS}	mm-ha	Derived fromHe et al. (2019) & MACA (Abatzoglou, 2013) using Walter et al. (2000)	County-level, annual

water) to the crops they chose to grow with the objective of maximizing farm-level NR subject to land and water constraints (Eq. B1). The constraints in Eq. B1 require that the total LU and WU for all crops in the region is less than or equal to the total land and water available for cultivation, as well as standard non-negativity constraints. The production function that simulates crop growth is a generalized constant elasticity of substitution (CES) production function that maps resource allocation (land and water) to PD (Eq. B2). Our model accommodates both irrigated and rainfed crops by separating water provided via precipitation (which is costless to the farmer) from water applied via supplemental irrigation (which does incur costs) (Maneta et al., 2020).

Water availability can be constrained by policy rules, or by physical water availability at diversion points as simulated by the hydrologic component. Limits on land availability can be restricted to less than the physical agricultural land in the county to simulate the effect of fallow on crop rotations or extend the available land to simulate double cropping (Fig. 2). A production function embedded in the economic model relates LU and WU to PD and is used in conjunction with information on production costs, crop prices, and water and land availability to calculate county-scale revenues.

The hydrologic and economic components interact through water diversions for supplemental irrigation. Seasonal WU calculated by the economic component for each crop is transformed into daily diversion rates according to the crop development state and irrigation and conveyance efficiency factors (Eq. B.4). These diversion rates are subtracted from streamflows at corresponding diversion nodes of the hydrologic network. Daily diverted water rates are proportionally redistributed over pixels marked as cropland in a predefined crop mask (Eq. B.3).

In total, there are eight inputs necessary to run the hydro-economic model (Table 1). The hydrologic component required precipitation and temperature data (Fig. B1). The economic component required data on natural crop water use (CWU, which we define as water consumed by crops not coming from supplemental irrigation), crop prices, variable unit costs of cultivating land, and cost of applying water (USDA NASS, 2017). Planting and harvesting dates used to calculate crop growth stage were derived from the U.S. Bureau of Reclamation (2016) AgriMet tables. Irrigation-system efficiencies were derived from MT DNRC (2017) data using Brouwer et al. (1989).

He et al. (2019) calculated baseline total water used by each crop from natural sources (CWU_{base}) from remote sensing data over fields known to be rainfed. End-of-century total natural crop water use (CWU_{eoc}) was estimated by adjusting CWU_{base} by the projected percent change in mean growing season aridity index ($\overline{AI}$). The growing season (April 1st – September 30th) used was chosen to be inclusive of the usual planting and harvesting dates reported by the USDA NASS (2010), and because irrigation water rights in Montana begin on April 1st of each growing season (MT DNRC, 2017). $\overline{AI}$ is defined as the ratio of mean growing season reference evapotranspiration ($\overline{ETr}$) to mean growing season precipitation ($\overline{P}$). $\overline{ETr}$ was calculated following the American Society of Civil Engineers (ASCE) standardized reference evapotranspiration (ETr) equation (Walter et al., 2000) using downscaled precipitation, temperature, relative humidity, and downwelling solar radiation grids from each of the considered GCMs within the MACA dataset. Wind velocity data was obtained from the gridMET dataset and used for all future $\overline{ETr}$ calculations due to the lack of wind velocity grids in the MACA datasets. For each GCM, future $\overline{ETr}$ was calculated for every 4 × 4 km resolution grid cell for every daily time-step over the entire 11-year end-of-century period, then aggregated at the county-scale for each growing season. CWU_{eoc} for each county, crop and scenario year was calculated as the difference between CWU_{base} and the inverse of $\overline{AI}$ multiplied by CWU_{base}. If the resulting CWU_{eoc} returned a value equal to or less than zero, then the CWU_{eoc} value was set to the minimum value greater than zero over all scenario years for that county and crop.

3.2. Spatial discretization of the hydrologic and economic models

Sub-catchments and the structure of the regional drainage network was generated using the USGS GTOPO30 digital elevation model (DEM) at 1 km resolution (USGS, 1996). The location of active USGS National Water Information System (NWIS) discharge gages were used to place the initial set of nodes to divide the model domain into sub-catchments (Maneta et al., 2020). Additional ungaged nodes were added to generate more sub-catchments and achieve the spatial detail that we considered adequate in resolving

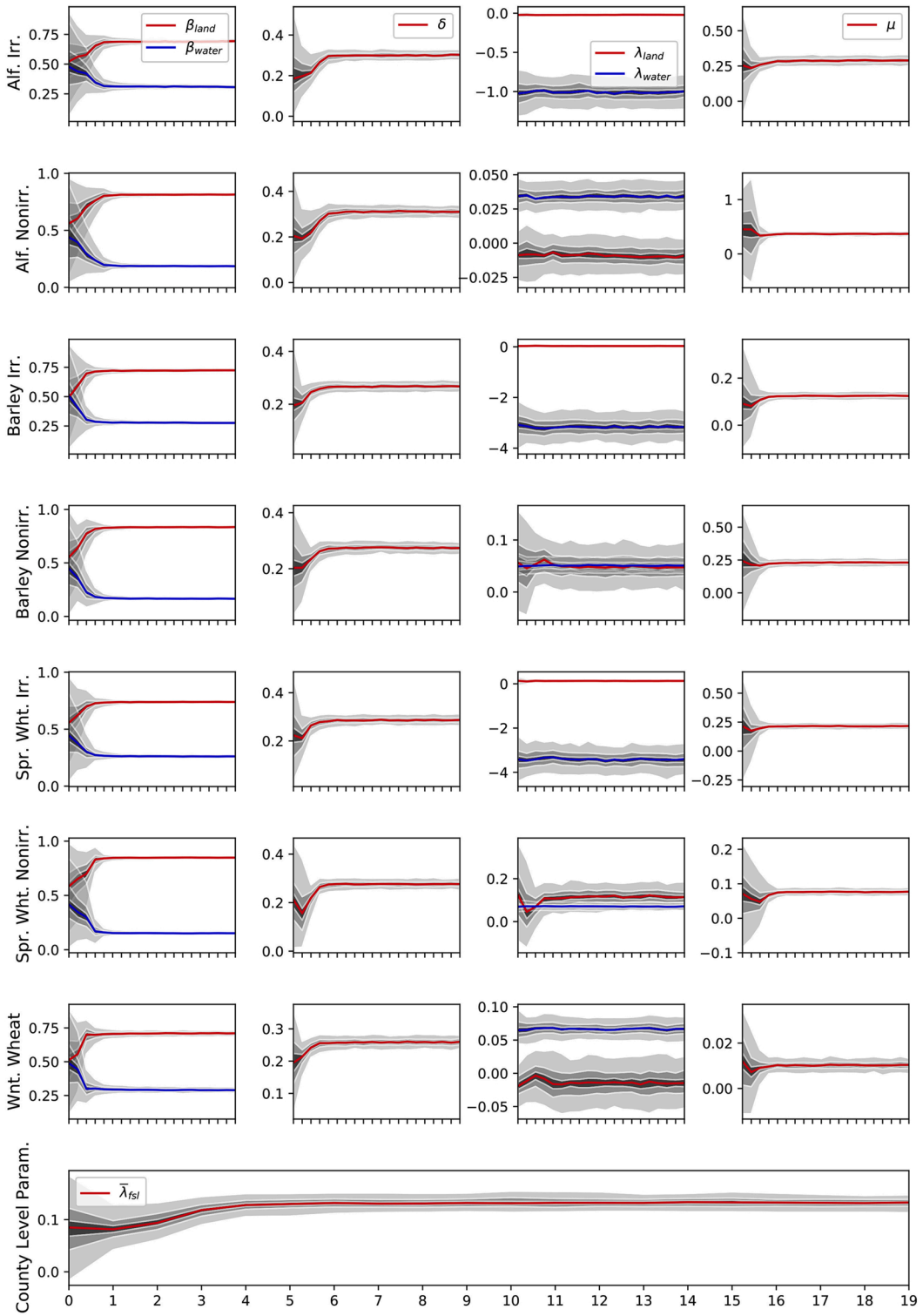

Fig. B1. Evolution of the parameter ensemble for 20 data assimilation periods during calibration in Beaverhead County. Shaded areas are the 95 and 68 percentile confidence intervals of the ensemble (form Maneta et al., 2020).

spatial variability of SF. The final hydrologic system model was represented with 330 sub-catchments. Each sub-catchment contains one river reach.

Montana's 56 counties were used as the spatial units for the economic component (Fig. 1b). Each economic unit (county) receives

Table A1
Hydrologic model parameters and calibrated values for the three clusters. Refer to technical appendices in Maneta et al. (2020) for a detailed description of the hydrologic component.

Parameter Name (units)	Parameter description	Cluster 1	Cluster 2	Cluster 3
pp_temp_thres (°C)	Precipitation temperature threshold	1.45	1.92	-0.74
ddf ($mm°C^{-1}d^{-1}$)	Degree day factor	3.58	2.65	4.92
soil_max_wat (mm)	Maximum soil water content	211.05	100.21	121.47
soil _beta (-)	Empirical soil routing coefficient	4.55	2.19	1.31
aet_lp_param (-)	Evapotranspiration limit	0.37	0.50	0.35
hbv_hl1 (mm)	Storage parameter for upper groundwater compartment (UZ)	3.84	71.82	15.43
hbv_ck0 (d^{-1})	UZ vadose zone conductance	3.75	1.75	14.37
hbv_ck1 (d^{-1})	UZ saturated zone conductance	14.24	25.22	8.33
hbv_ck2 (d^{-1})	Lower groundwater compartment (LZ) conductance	8861.34	3183.61	4959.04
hbv_perc (d^{-1})	Percolation from UZ to LZ	22.87	13.37	27.53
hbv_pbase (h)	River routing transformation routine parameter	4	4	4
K (d)	Muskingum-Cunge parameter controlling the celerity of wave routing through the channel	83,265.77	86,481.24	84,027.74
e (-)	Muskingum-Cunge parameter controlling the dispersion of wave routing through the channel	0.52	0.50	0.50

irrigation water from one node of the stream network (termed diversion nodes) selected from the river reach that passes through the county.

3.3. Model calibration datasets and procedures

3.3.1. Hydrologic component calibration

The hydrologic model (HBV + Muskingum-Cunge) has a total of 13 hydrologic component parameters, which were calibrated using the brute-force Monte Carlo method on 32 pilot sub-catchments, each containing a USGS NWIS discharge gage and a USDA Natural Resources Conservation Service (NRCS) Snow Telemetry (SNOTEL) station. The current version of the model cannot simulate the effect of reservoirs. Because of this limitation we vetted the USGS NWIS gage locations and selected those not impacted by reservoirs. This process resulted in the 32 pilot sub-catchments used for calibration. Calibration was done against 10-year historical (2009–2018) USGS NWIS discharge gage and SNOTEL stations data using the Kling-Gupta Efficiency (KGE) statistical metric (Gupta et al., 2009) as the objective function. Historical precipitation and air temperature data used during hydrologic model calibration was obtained from the gridded meteorological database (gridMET) (Abatzoglou, 2013). The 330 sub-catchments in the domain were grouped by similarity using a K-Means clustering analysis (Hartigan & Wong, 1979) based on eight catchment descriptors: total area, stream gradient, stream length, percent land use (agriculture, forest, grassland, urban), and mean percent clay in upper soil (0–150 cm). Catchment areas and stream descriptors were calculated from the GTOPO30 DEM using GIS procedures. Land use and soil classification descriptors were obtained from the USDA NRCS Soil Survey Geographic Database (SSURGO) (Soil Survey Staff, 2018). The optimum number of clusters was determined using a silhouette plot (Rousseeuw, 1987) and each of the 330 sub-catchments was grouped into one of three clusters. Cluster 1, 2 and 3 included 2, 28, and 2 of the 32 pilot sub-catchments, respectively. Cluster 2 contained a majority of the headwater sub-catchments, which have less probability of being impacted by reservoirs and contain the most SNOTEL stations. This explains the disproportionate number of pilot sub-catchments in cluster 2. The pilot sub-catchments assigned to each cluster were calibrated using 10,000 brute-force Monte Carlo simulations using 10-year (2009–2018) historical daily input time series of snow water equivalent and streamflow. At the conclusion of the Monte Carlo simulations, the set of parameter values from the model run that achieved the best combined (USGS NWIS and SNOTEL data) KGE value was used as the parameter set for all sub-catchments within the same cluster. Table A1 provides additional details on the parameters of the hydrologic component.

3.3.2. Economic component calibration

The economic component was calibrated in a previous study using a using recursive Bayesian filter (Maneta et al., 2020). The calibration was done independently of the hydrologic model and involved ingesting historical (2008–2018) information of production costs and crop prices, and remote sensing observations of area planted, crop type, crop yields, and crop evapotranspiration (as an approximation of crop water use) to determine the parameters of Eq. (B1). Under the assumption that resource allocation is driven by maximizing profit, past observations of LU and WU to each crop *i* are solutions to the objective function that maximizes farm NR (Eq. (B1)). The calibration of the economic component using the Bayesian filter yields the probability distribution of parameter values that satisfy the first- and second-order conditions that solve Eq. (B1) for a maximum at the observed probability distributions of LU, WU, and PD. The nonlinear optimization program that solves Eq. (B1) treats the model parameters as an ensemble of stochastic variables that are recursively adjusted by the sequence of agricultural observations using a recursive Bayesian filter. The result of the process is an ensemble of parameters conditioned to the history of observations of LU and WU in each economic unit (county). An example of the dynamics of the model parameter ensemble for one county is provided in Fig. (B1). The range in the values of the parameter ensemble approximates the probability distribution of optimal parameters given the uncertainty of the historical observations. In this analysis we reconstructed the probability distribution of each parameter using ensembles sizes of 300 members. Description of the economic component's data sources is provided in Appendix C.

3.4. Model application

The application of our calibrated hydro-economic model for Montana compares end-of-century climate change projections (2080–2090) from hindcast (2008–2018) conditions simulated by five downscaled global climate models (GCMs) under the high-risk RCP 8.5 carbon emissions scenario. Our analysis assumes that no new crop types including genetically modified varieties are introduced in the future, no new technologies that affect irrigation efficiency, no new sources of available water, and now new agricultural policies that alter the amount of water farmers can legally access. Under these projections and assumptions our results represent the net impact of on-farm adaptation strategies when no other mitigating action is taken. Our aim was to isolate the hydro-economic effects of farmers' adaptive behavior in response to climate change. This scenario provides water resource managers and policy makers a worst-case limit on the economic impacts of climate on agriculture.

3.4.1. Climate and economic scenarios

Baseline (2008–2018) and end-of-century (2080–2090) climatological daily precipitation and temperature datasets needed to run the model were drawn from a 4 × 4 km gridded statistical downscaling of five GCM outputs using the Multivariate Adaptive Constructed Analogs (MACA) method (Abatzoglou, 2013). The five GCMs chosen for this study (Supplementary Material Table D.1) were participants in the Coupled Model Intercomparison Project 5 (CMIP5) and were chosen based on their overall low relative error simulating historical mean temperature and precipitation in the U.S. Pacific Northwest (Rupp et al., 2013). Each of the five GCMs provides a climate scenario with 11 years of historical baseline data and 11 years of end-of-century data.

To represent economic conditions, we used 11 years, 2008–2018, of agricultural market observations of crop prices and production costs. Each year was considered an independent economic scenario with mean crop prices and input costs equal to the observed value each year and a common variance equal to the variance of the data during the 11-year record.

For each climate scenario and period, the hydro-economic model was run 11 times, once for each of the 11 economic scenarios. This generated 121 years of hydro-economic information (11 years of GCM simulation x 11 agricultural market scenarios) for each of the five GCMs and each of the periods (baseline and end-of-century). Section 3.4.3 describes how the ensemble was processed to reconstruct the final model forecast probabilities.

3.4.2. Model spin-up

For each GCM and each climate scenario the model was spun-up by rerunning the hydrologic component enough times to allow the HBV water storage compartments to achieve steady-state conditions. Then, for each of the 11 economic scenarios, the spun-up hydro-economic model was spun-up once more by running one full cycle through all 11 climate scenario years. This step permits the hydrologic model to stabilize again under the new economic scenario. Once these spin-up runs were completed, the model was run again, and model results were collected for analysis.

3.4.3. Propagation of model uncertainties and reduction of forecast ensembles

The stochastic nature of our hydro-economic model permits to propagate uncertainties from different sources used and generates probabilistic forecasts of SF, WD, LU, WU, PD, and NR for the 56 counties of the state of Montana. The uncertainty in any single model forecast reflects the uncertainty from the economic model parameters, which in turn reflects the uncertainty in the observations of agricultural activity used to calibrate the model, as well as the uncertainty associated with the interannual variability of precipitation and potential evapotranspiration, and the interannual variability of crop prices, production costs, and water available for irrigation. The final ensemble of model forecasts also reflects the uncertainty associated with the spread in climate model projections (disagreements between GCMs). The model forecasts do not consider the effect of uncertainties in the hydrologic model parameters due to computational limitations; however, SF forecasts reflect uncertainties associated with interannual variability of precipitation and evapotranspiration as well as the effects of the spread (disagreements) between climate models. The way we have handled uncertainty and aggregated the ensemble of model simulations is described here.

To represent the total uncertainty in the system associated with climate and economic variability and with GCM projection disagreements we run all combinations of economic and climate scenarios from 5 GCMs resulting in 605 simulated years (11 years of climate records per period x 11 economic scenarios x 5 GCMs) per period (baseline and end-of-century). These 605 simulated years span the range of precipitation, temperature, natural crop evapotranspiration, and agricultural market conditions of the baseline and forecast periods including variations associated with GCM disagreements.

Total uncertainty in the forecasts of daily SF and WD for each period was obtained by stacking the 605 years to generate an ensemble of daily SF and WD. We used this ensemble to approximate the probability distribution of daily SF and WD each period and to calculate the probability distribution of relative change between them. These ensembles represent the interannual variability in each climate scenario (GCM), the variability between GCMs, and the variability induced by varying WD associated with farmer adaptation to the economic and climatic conditions. The effect of the uncertainty in the hydrologic parameters was not factored in.

Total uncertainty in the forecasts of LU, WU, PD, and NR for each crop and county were calculated differently. This is because these forecasts are annual, and because for each of the 605 simulated years in each period the economic component also produced a 300-member ensemble forecast that reflect the uncertainty in the calibrated economic model parameters. To reduce the size of the ensemble we calculated the median of each ith member across all 605 simulated years in each period and used the resulting consolidated ensembles in each period to calculate the ensemble of relative change in these variables between baseline and end-of-century.

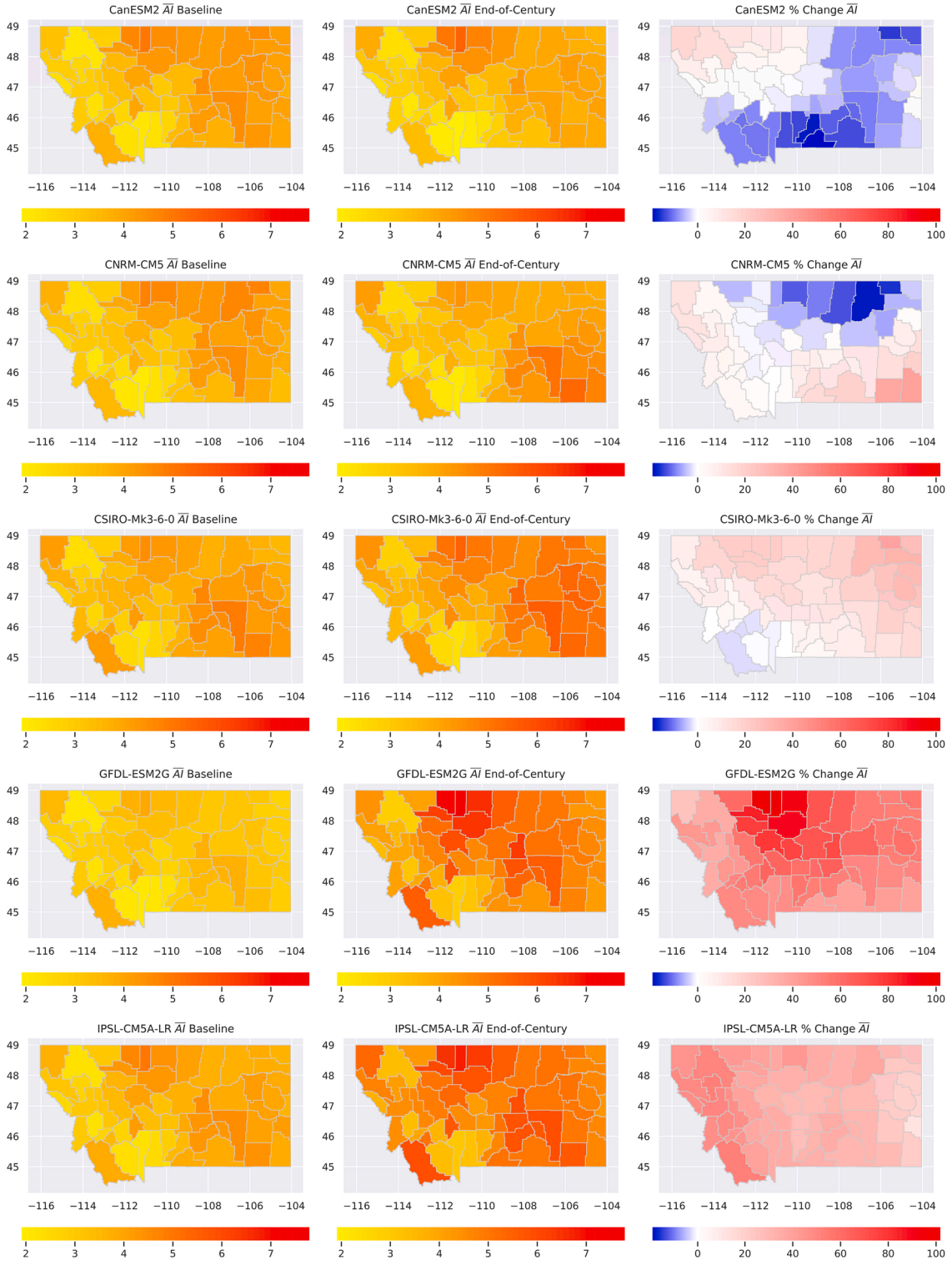

Fig. 3. Global climate models (rows) county-scale mean growing season aridity index for baseline (left), end-of-century (center), and percent change between baseline and end-of-century (right).

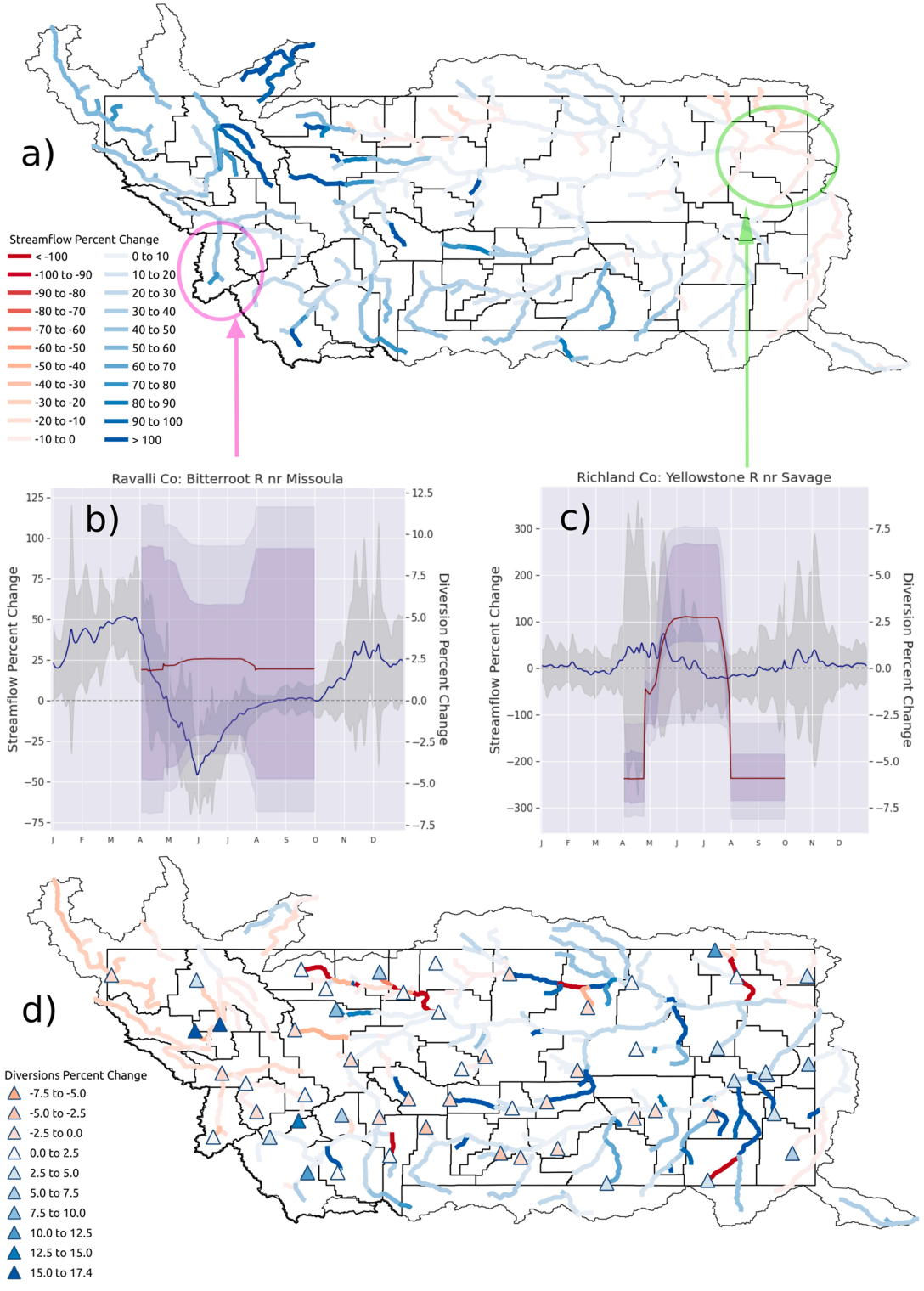

(caption on next page)

Fig. 4. a) Mean percent change in streamflows over the winter (January - March). Ravalli County highlighted by the pink oval, Richland County highlighted by the green oval. Hydrograph of the dominant river segment for b) Ravalli and c) Richland counties. Primary y-axis: Mean percent change in streamflow between baseline and end-of-century climate projections (blue line), grey shading indicating 95% uncertainty envelope associated with interannual climate variability and climate model error. Secondary y-axis: Mean percent change in water diversions for irrigated agriculture between baseline and end-of-century projections (red line), magenta shading indicating the 0.45–0.55 and 0.4–0.6 uncertainty range of modeled diversions. d) Mean percent change in streamflows over the spring (April - June). Symbols represent the maximum value of the mean percent change in water diversions over the growing season.

4. Results

4.1. Changes in climate aridity

All five GCMs agreed mean growing season average temperature ($\overline{T_{avg}}$) would increase by end-of-century and that the western portion of the state would increase more than the eastern portion, on a percent change basis (Supplementary Material Fig. D.1). Among all five GCMs $\overline{T_{avg}}$ was expected to increase 31% state-wide. There was little model agreement in end-of-century $\overline{P}$. The CanESM2 model projected increased $\overline{P}$ state-wide, the GFDL-ESM2G model projected decreased $\overline{P}$ state-wide, and the other three models projected regional changes, none of which agreed on spatial patterns (Supplementary Material Fig. D.2). Among all five GCMs $\overline{P}$ was expected to increase 4.9% state-wide. All five GCMs agreed $\overline{ETr}$ would increase state-wide, but there was little spatial agreement on which regions would experience the largest percent change (Supplementary Material Fig. D.3). Among all five GCMs $\overline{ETr}$ was expected to increase 20% state-wide.

As with $\overline{P}$, there was little model agreement in end-of-century $\overline{AI}$ (Fig. 3). Among all five GCMs $\overline{AI}$ was expected to increase 21% state-wide. The most extreme end member GCMs were the GFDL-ESM2G and CanESM2 models. The GFDL-ESM2G model projected a 57% state-wide increase in $\overline{AI}$. However, the CanESM2 model projected a 3.5% state-wide reduction in $\overline{AI}$, albeit with high spatial variability and some counties showed an increase. The only spatial uniformity among all five GCMs was in the northwest counties, where all projected increased $\overline{AI}$. Although there was little spatial agreement among the GCMs, the magnitude of projected changes was important. As indicated on the colorbar in Fig. 3, the range across all GCMs spanned − 19–102%. The CanESM2 model was balanced, ranging from − 19–17%, but the other models were unbalanced towards more arid conditions by the end of the century.

4.2. Water diversions and water use

The overarching result in SF projections from our model align with previous studies that analyzed streamflow variations in the western U.S. (Bales et al., 2006; Das et al., 2011; Li et al., 2017; McCabe and Clark, 2005; Pederson et al., 2011; Rauscher et al., 2008; Regonda et al., 2005). Further hydrology results analysis and hydrographs for all counties are provided in Supplementary Material (Appendix E).

Projected changes in total WD for irrigated agriculture showed a high level of uncertainty, both statistically and spatially. Ravalli County for instance is a productive irrigated region that relies on water from the Bitterroot River (Fig. 4b). Simulated mean total WD for agriculture in the Bitterroot River intensified by approximately 2.4% throughout the growing season, but projections showed a very large spread that reflected both the uncertainty in the economic model parameters and the disagreements in $\overline{P}$ and $\overline{AI}$ among the GCMs. The majority of counties (63%) projected an increase in the maximum mean percent change in WD (Fig. 5a). The dominant temporal trend in mean total WD showed lower changes in the early and late growing season and higher changes in the middle portion when crops were in full coverage and irrigation requirements were higher (Figs. 4b, c, 5b & c).

Overall average state-wide median projections in WU showed a slight decrease for irrigated alfalfa, and large increases for irrigated barley and irrigated spring wheat (Table 2); therefore, collectively our results projected increased total WU for the state. The spatial patterns of median percent change in WU showed increases for irrigated alfalfa across the majority of counties in the northwest and southwest regions, slight changes (both positive and negative) in the central region, and predominantly decreases across the rest of the state (Fig. 6a). As a whole, less than half of the counties increased WU for irrigated alfalfa (29%). The majority of counties projected increased WU for irrigated barley (73%); however, the Gallatin (southwest region), Marias (central region) and most of the lower Missouri river corridor counties (central and northeast regions) projected slight decreases (Fig. 6b). The vast majority of counties projected increased WU for irrigated spring wheat (95%), with the western and eastern ends of the state projected to increase the most (Fig. 6c).

Table 3 shows the regional average values of projected changes in WU for each irrigated crop type. Projections showed the northwest and southwest regions to increase WU for irrigated alfalfa, while the other five regions all projected decreases. The

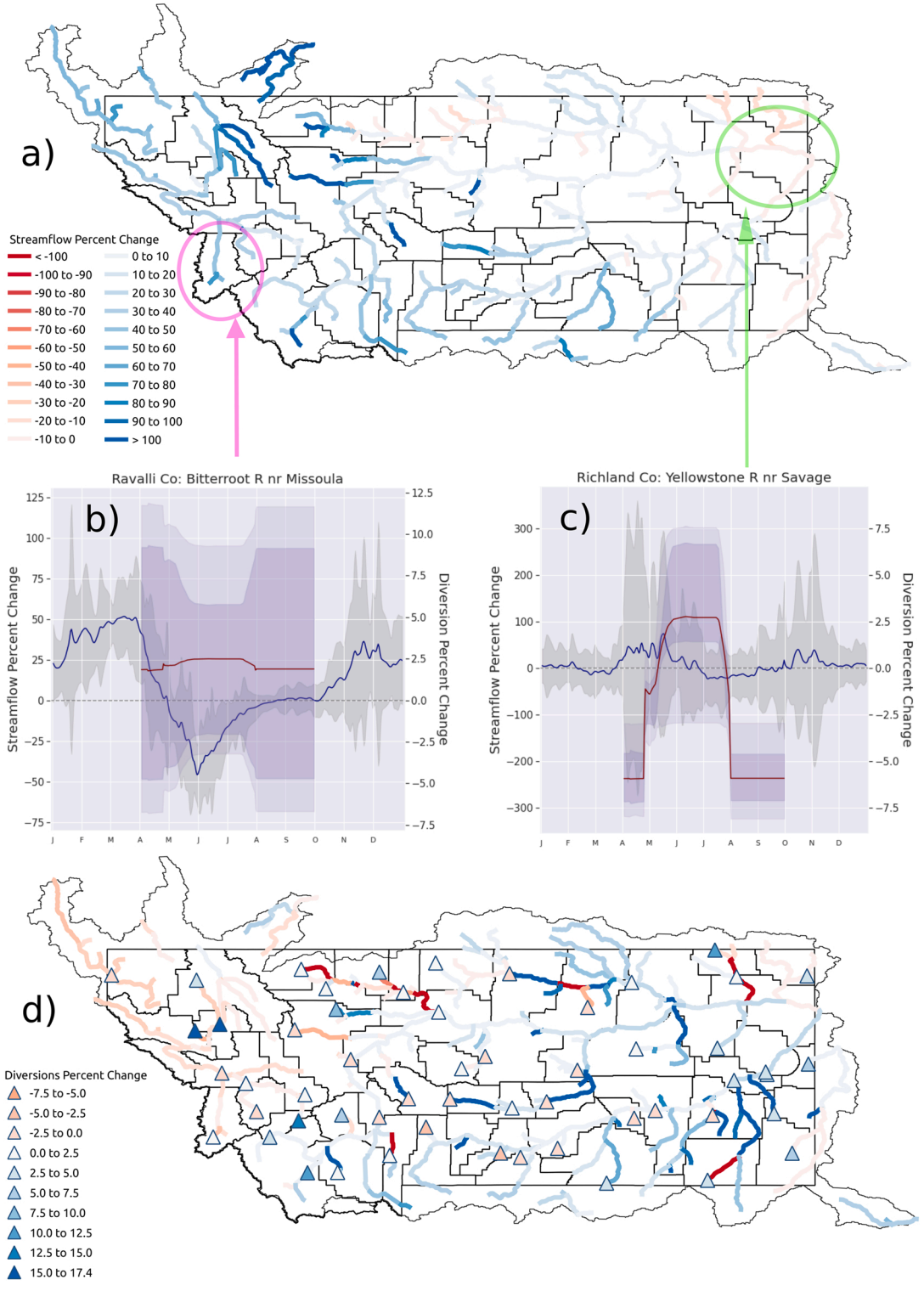

(caption on next page)

Fig. 5. a) Mean percent change in streamflows over the summer (July - September). Powell County highlighted by the pink oval, Phillips County highlighted by the green oval. Hydrograph of the dominant river segment for b) Powell and c) Phillips counties. Primary y-axis: Mean percent change in streamflow between baseline and end-of-century climate projections (blue line), grey shading indicating 95% uncertainty envelope associated with interannual climate variability and climate model error. Secondary y-axis: Mean percent change in water diversions for irrigated agriculture between baseline and end-of-century projections (red line), magenta shading indicating the 0.45–0.55 and 0.4–0.6 uncertainty range of modeled diversions. d) Mean percent change in streamflows over the fall (October - December). Symbols represent the maximum value of the mean percent change in water diversions over the growing season.

northwest and southwest regions have more abundant water, and closer sources of water, reducing total irrigation costs. Farms and ranches outside of the northwest and southwest regions are larger in area, with nearby water sources less abundant, which historically resulted in lower adoption of irrigation infrastructure due to the high cost of installation and water conveyance. These factors, as well as wheat and barley being more dominant in other regions, resulted in the northwest and southwest regions prioritizing and intensifying irrigated alfalfa. The other regions prioritized irrigated barley and spring wheat (Fig. 6a & 6c). Historically, the southwest region devoted the most land to irrigated alfalfa, and our projections showed the largest change in WU for irrigated alfalfa in that region. The north central and southwest regions were the largest producers of irrigated barley and our projections showed increased WU. The northwest region was projected to have the largest change in WU for irrigated barley, which resulted from the low acreage of irrigated barley grown in the region historically; therefore, the comparatively small increase in the volume of irrigation water translated into the large percent change in WU. The northeast region projected the largest increase in WU for irrigated spring wheat, more than two times the state-wide average. Likewise, the northwest region projected significantly increased WU for spring wheat. All seven regions projected increased WU for irrigated barley and spring wheat.

4.3. Land allocations

On the state-wide- and regional-scale, average values of the median percent changes in LU to all non-irrigated crops were projected to decrease (Table 2 & 4). That decrease applied to the majority of the state, with a small number of counties (two to six) projected to increase LU for non-irrigated crops (Fig. 7b, d, f, & g). Conversely, average state-wide projections showed increased LU for all irrigated crops (Table 2). Regionally, irrigated alfalfa projected mixed spatial results (four of seven regions projected increases), irrigated barley projected increases in all regions, and irrigated spring wheat projected increases in all but the north central region (Table 4). There was no distinct spatial pattern in LU for irrigated crops (Fig. 7a, c, & e), but the majority of counties increased LU for irrigated barley and irrigated spring wheat (66%) and less than half of the counties increased LU for irrigated alfalfa (43%).

4.4. Crop production

Not all counties that increased LU and/or WU increased PD (Fig. 8). For irrigated alfalfa only seven counties showed increased PD (Fig. 8a), and all seven increased both LU and WU (Fig. 7a & 6a, respectively). Twenty counties showed increased PD of irrigated barley (Fig. 8c), all of which increased LU (Fig. 8c), but only 16 of those 20 increased WU (Fig. 7b). Fifty-three counties increased WU for irrigated spring wheat, but only 19 increased PD (Fig. 8e) and all 19 increased both LU and WU (Fig. 7e & 6c, respectively). Only Sheridan County increased PD of any non-irrigated crop, and only for winter wheat (Fig. 8g). Sheridan County increased LU for winter wheat by 10.3% (Fig. 7g) but only increased PD by 0.5%. Regionally, only the southwest region projected increased PD (for both irrigated barley and irrigated spring wheat) (Table 5). State-wide, average projections showed decreased PD of all crops (Table 2).

4.5. Farm net revenue

Taking into account all predicted changes in LU, WU, and PD, only 20 of 56 counties projected increased NR across any crops (Fig. 9). Regionally, only irrigated barley in the southeast region projected an increase in NR (Table 6). Historically, the southeast region grew significantly less irrigated barley (and therefore used less water) than the other regions. Model results showed the southeast region would increase LU for irrigated barley by 8.0% (Table 4), increase WU by 19.2% (Table 3), which only resulted in a 0.8% increase in NR (Table 6). Overall average state-wide projections showed decreased NR for all crops, and all non-irrigated crops decreased more than any irrigated crop (Table 2).

4.6. Projection uncertainty of resource allocation

In order to convey the uncertainty in the model results, the probability distributions of economic variables for each crop type in

Table 2
Statewide average values of the projected median percent change for each crop type and economic variable. Total range given in parentheses.

	Irrigated Alfalfa	Non-irrigated Alfalfa	Irrigated Barley	Non-irrigated Barely	Irrigated Spring Wheat	Non-irrigated Spring Wheat	Winter Wheat
Water Use	-1.0 (−15.8 to 27.1)	N/A	17.4 (−7.2 to 164.4)	N/A	38.1 (−8.9 to 257.8)	N/A	N/A
Land Use	0.5 (−6.6 to 33.6)	-8.6 (−19.2 to 4.3)	2.8 (−4.0 to 25.0)	-6.0 (−12.8 to 2.7)	1.5 (−4.6 to 14.1)	-6.1 (−13.0 to 1.4)	-5.1 (−12.2 to 11.4)
Production	-1.1 (−3.5 to 3.4)	-3.2 (−11.3 to −1.2)	-0.2 (−1.9 to 4.1)	-2.6 (−6.8 to −0.1)	-0.2 (−2.9 to 2.1)	-2.4 (−6.6 to −0.3)	-2.4 (−7.0 to 0.5)
Net Revenue	-2.5 (−8.2 to 15.9)	-9.2 (−16.3 to −5.1)	-0.8 (−7.0 to 7.0)	-6.7 (−14.3 to −2.3)	-1.3 (−5.9 to 3.6)	-6.9 (−11.2 to −3.6)	-6.1 (−9.9 to 1.7)

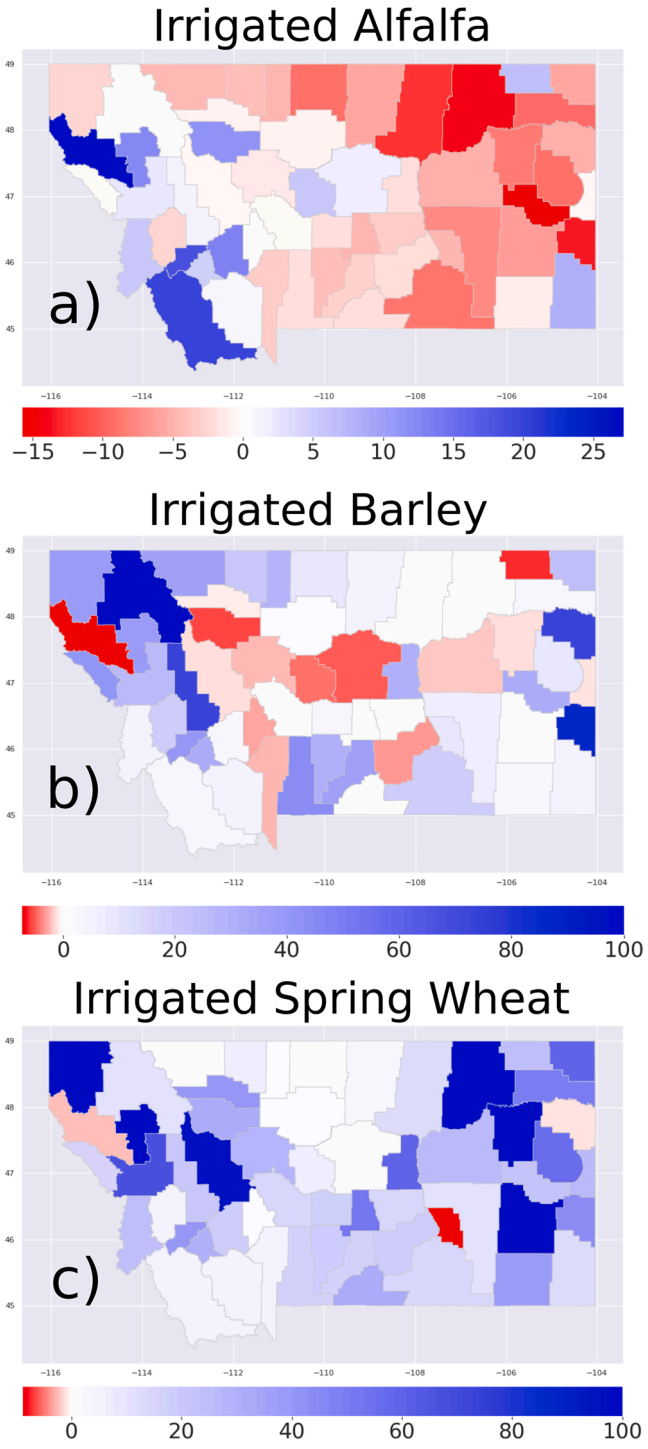

Fig. 6. County-scale median percent change (across all model climatic and economic scenarios) between the baseline (2008–2018) and end-of-century (2080–2090) projections. Different color scales for each crop type.

Table 3
Regional average values of the projected median percent changes in water allocated to each irrigated crop type. Total range given in parentheses.

	Irrigated Alfalfa	Irrigated Barley	Irrigated Spring Wheat
Northwest	6.2 (−2.7 to 27.1)	43.8 (−7.2 to 164.4)	63.0 (−2.4 to 255.6)
Southwest	7.1 (−3.2 to 20.1)	8.4 (−2.2 to 32.4)	13.0 (4.4–31.0)
North Central	-3.4 (−12.4 to 11.3)	10.8 (−5.3 to 37.3)	11.1 (0.8–39.8)
Central	-0.7 (−4.8 to 5.7)	2.1 (−4.7 to 31.1)	29.7 (1.3–97.1)
South Central	-3.8 (−8.7 to −1.9)	19.5 (−3.0 to 43.8)	15.8 (−8.9 to 33.3)
Northeast	-6.3 (−14.0 to 6.5)	12.9 (−5.9 to 73.6)	81.3 (−1.0 to 257.8)
Southeast	-5.2 (−15.8 to 8.2)	19.2 (−0.7 to 87.1)	39.7 (10.2–124.2)

Ravalli and Richland counties are presented here (Fig. 10 and 11, respectively). The probability distributions for all counties are presented in Supplementary Material (Appendix F). Ravalli County was chosen as representative of the Northern Rockies region because it has large LU and WU devoted to irrigated agriculture and model results showed increased WU for all irrigated crops. Richland County was chosen as representative of the NGP region because it has the most LU for irrigated spring wheat in the state. Even with our methodology of producing the aggregated ensembles, the LU and WU distributions in both counties spanned large projected changes and zero percent change was within the 95% confidence interval. The changes in WU distributions were skewed right (Figs. 10 & 11), signifying modestly higher probabilities of large increases in WU for irrigation. The probability distributions of the change in PD were quite narrow. These narrow changes in PD probability distributions did not directly translate to narrow changes in NR probability distributions. As with the changes in LU and WU probability distributions, the change in PD and NR probability distributions spanned zero percent change, which lies within the 95% confidence interval. The uncertainty around these values was largely due to the model's response to the different climate projections represented by the GCMs, but also incorporated the effects of parameter uncertainty in the economic component.

5. Discussion

5.1. Climate change uncertainty

Differences in the GCMs' projections of $\overline{P}$ contributed to the large potential range of hydro-economic outcomes across Montana, as evidenced by large uncertainty envelopes around SF and WD changes, spatial and magnitude uncertainty in $\overline{AI}$, and wide probability distributions for LU, WU, PD, and NR. Projections of precipitation changes across the western U.S. were similarly uncertain (U.S. Global Change Research Program (2017)) which makes water resource management planning difficult (Groves et al., 2008; Tanaka et al., 2006). Conversely, there was agreement that temperatures will increase in Montana and across the western U.S. (U.S. Global Change Research Program (2017)). Increased temperatures can impact agricultural productivity in numerous ways. For example, optimal crop growth occurs within specific intermediate temperature intervals and excessive heat is detrimental to physiological processes which therefore decrease crop yield (Anderson, 2016; Schauberger et al., 2017). On the other hand, warmer spring temperatures may allow for earlier planting dates which could increase crop productivity (Lanning et al., 2010), but at the risk of damaging frosts (Kim et al., 2014). While increasing temperatures could impact crop production, the aridity index might be a better proxy for the viability of future agricultural productivity (Paltasingh et al., 2012); however, the complexities of plant water use efficiency of photosynthesis with changing atmospheric CO_2 concentrations has been shown to alter relations between hydrology and ecology parameters (Greve et al., 2019; Roderick et al., 2015).

Future modeled projections of changes in annual aridity index showed increasing trends (more arid conditions) across most of the western U.S. (Ficklin & Novick, 2017; Fu & Feng, 2014; Scheff & Frierson, 2015; Sherwood & Fu, 2014). While our results did show disagreements in end-of-century $\overline{AI}$ among the five GCMs, the overall magnitude of change after aggregating all projections indicated more arid conditions by the end of the century. The more arid conditions were driven by increased atmospheric evaporative demands, i.e., increased $\overline{ETr}$ (Supplementary Material Fig. D.3). Wurster et al. (2020) examined historic (1979–2016) ETr, price and precipitation anomalies impact on crop production in Montana and surrounding states. Their results highlighted that alfalfa production was

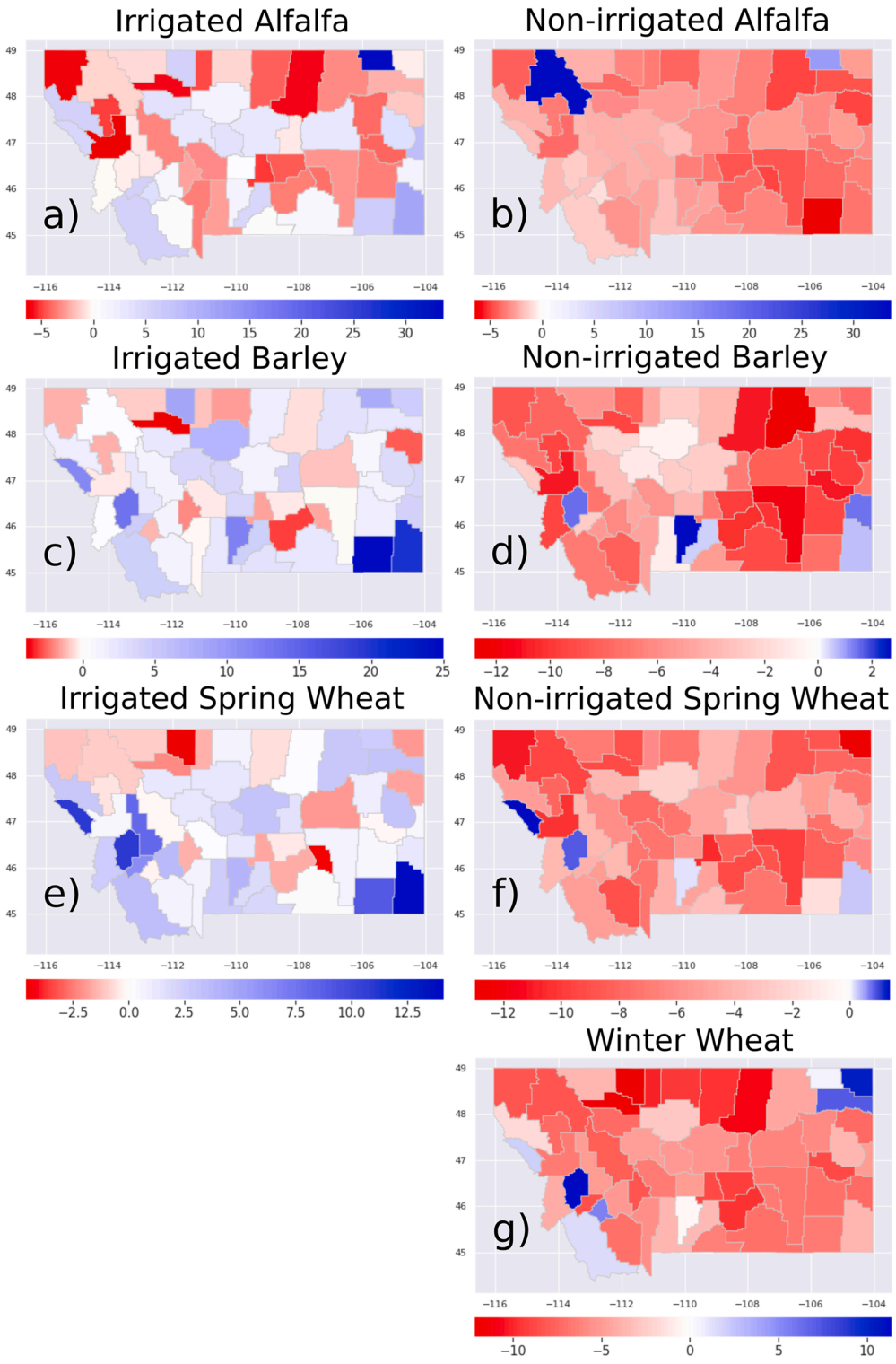

Fig. 7. County-scale median percent change (across all model climatic and economic scenarios) between the baseline (2008–2018) and end-of-century (2080–2090) projections. Different color scales for each crop type.

most sensitive to ETr anomalies across the majority of Montana, although irrigation largely decoupled alfalfa production from climate

Table 4
Regional average values of the projected median percent changes in land allocated to each crop type. Total range given in parentheses.

	Irrigated Alfalfa	Non-irrigated Alfalfa	Irrigated Barley	Non-irrigated Barely	Irrigated Spring Wheat	Non-irrigated Spring Wheat	Winter Wheat
Northwest	-0.4 (−6.6 to 5.8)	-6.1 (−12.0 to 4.3)	3.1 (−1.3 to 13.6)	-6.4 (−10.9 to 1.5)	4.0 (−1.1 to 11.0)	-5.4 (−11.0 to 1.4)	-3.6 (−8.4 to 11.4)
Southwest	1.5 (−3.4 to 5.5)	-5.9 (−8.5 to −2.3)	1.1 (−1.2 to 4.3)	-6.3 (−8.2 to −4.9)	1.8 (−0.2 to 3.8)	-6.2 (−9.1 to −3.8)	-2.1 (−7.0 to 5.6)
North Central	-1.3 (−5.9 to 5.5)	-9.4 (−12.0 to −6.4)	1.3 (−4.0 to 8.5)	-5.3 (−10.8 to −0.7)	-0.7 (−4.6 to 1.4)	-6.1 (−9.3 to −2.5)	-8.7 (−12.2 to −2.7)
Central	-0.9 (−5.1 to 3.6)	-8.4 (−12.8 to −5.2)	1.4 (−2.0 to 4.1)	-4.8 (−9.8 to −1.1)	0.6 (−1.7 to 3.3)	-6.8 (−10.6 to 2.5)	-6.7 (−9.1 to −4.9)
South Central	-0.3 (−3.8 to 4.8)	-9.1 (−14.2 to −5.1)	2.7 (−3.0 to 12.0)	-4.6 (−10.3 to 2.7)	0.7 (−4.4 to 3.9)	-5.4 (−9.3 to 0.1)	-5.3 (−9.5 to −0.3)
Northeast	3.6 (−4.0 to 33.6)	-9.1 (−14.2 to 1.7)	2.3 (−2.6 to 8.2)	-8.4 (−12.8 to −3.3)	0.9 (−2.0 to 3.3)	-7.4 (−13.0 to −3.7)	-1.2 (−7.4 to 10.3)
Southeast	2.5 (−4.1 to 11.5)	-12.1 (−19.2 to −9.1)	8.0 (−0.1 to 25.0)	-6.4 (−11.5 to 1.4)	3.7 (−0.1 to 14.1)	-5.5 (−9.7 to 0.3)	-6.4 (−8.6 to −3.6)

conditions. Winter wheat production in the western and eastern border counties were most sensitive to ETr anomalies. Maxwell et al. (2017) stated the possibility of a transition to winter wheat from spring wheat as a result of warmer winter temperatures. Our results did not match the Maxwell et al. (2017) prediction and evidence of that transition was not observed in the 2008–2018 USDA NASS data. As new observations of agricultural activity become available our hydro-economic model may capture that transition if present.

5.2. Land use and water use

In Montana and throughout the Intermountain West, agricultural lands are still prevalent in counties that are rapidly urbanizing. Adjacent to and upstream of more urban counties are counties dominated by farming and ranching. For example, Missoula County is rapidly urbanizing, agricultural water demands are decreasing, but projected upstream intensification of agricultural WD in Ravalli and Powell counties (Fig. 4b & 5b, respectively) would impact Missoula's available water supply. Increases in agricultural water demand could amplify climate change impacts on summer SF. This is especially true in western Montana where our results showed summer SF would decrease (Fig. 4b & 5b). While the certainty around summer SF decreasing in the eastern plains were less conclusive, the majority of counties in the central and north central region projected slight decreases in maximum WD, but these regions still showed decreasing SF (Fig. 5a). Climate projections play a role, but upstream increases in WU could be the more significant translation of downstream water shortages. Therefore, the decisions farmers make in the headwater counties could have significant impact on counties situated downstream. Continuing historical trends experienced in the western U.S., end-of-century projected decreases in snowpack, growing season SF quantities, and shifts to earlier peak spring runoff (Bales et al., 2006; Das et al., 2011; Li et al., 2017; McCabe & Clark, 2005; Pederson et al., 2011; Rauscher et al., 2008; Regonda et al., 2005; Udall and Overpeck, 2017) will add further stress to agricultural water demands (Cross et al., 2017; Pathak et al., 2018). $\overline{T_{avg}}$ was projected to increase more in the mountainous western portion of Montana (Supplementary Material Fig. D.1), which is where the majority of irrigation takes place (MT DNRC, 2014). Increasing temperatures could require increased irrigation to avoid crop stress and counteract increased evaporation (Asseng et al., 2013; Döll, 2002; Fischer et al., 2007; Xiao et al., 2005). There is little room for increased surface water diversions from any basin across the state as the percentage of basin totals are already diverted at 95% or greater (MT DNRC, 2014).

5.3. Adaptation strategies

Our methodology considers a limited set of the adaptation strategies available to farmers, e.g., farmers could only change LU and/or WU but not change irrigation technology or introduce new crop varieties. Combining that with the variations in farming costs and crop market prices resulted in considerable noise surrounding our predictions of farmers' response to climate change. Medellín-Azuara et al. (2011) isolated how land and water allocations, crop prices, and agricultural revenues in California would change under a

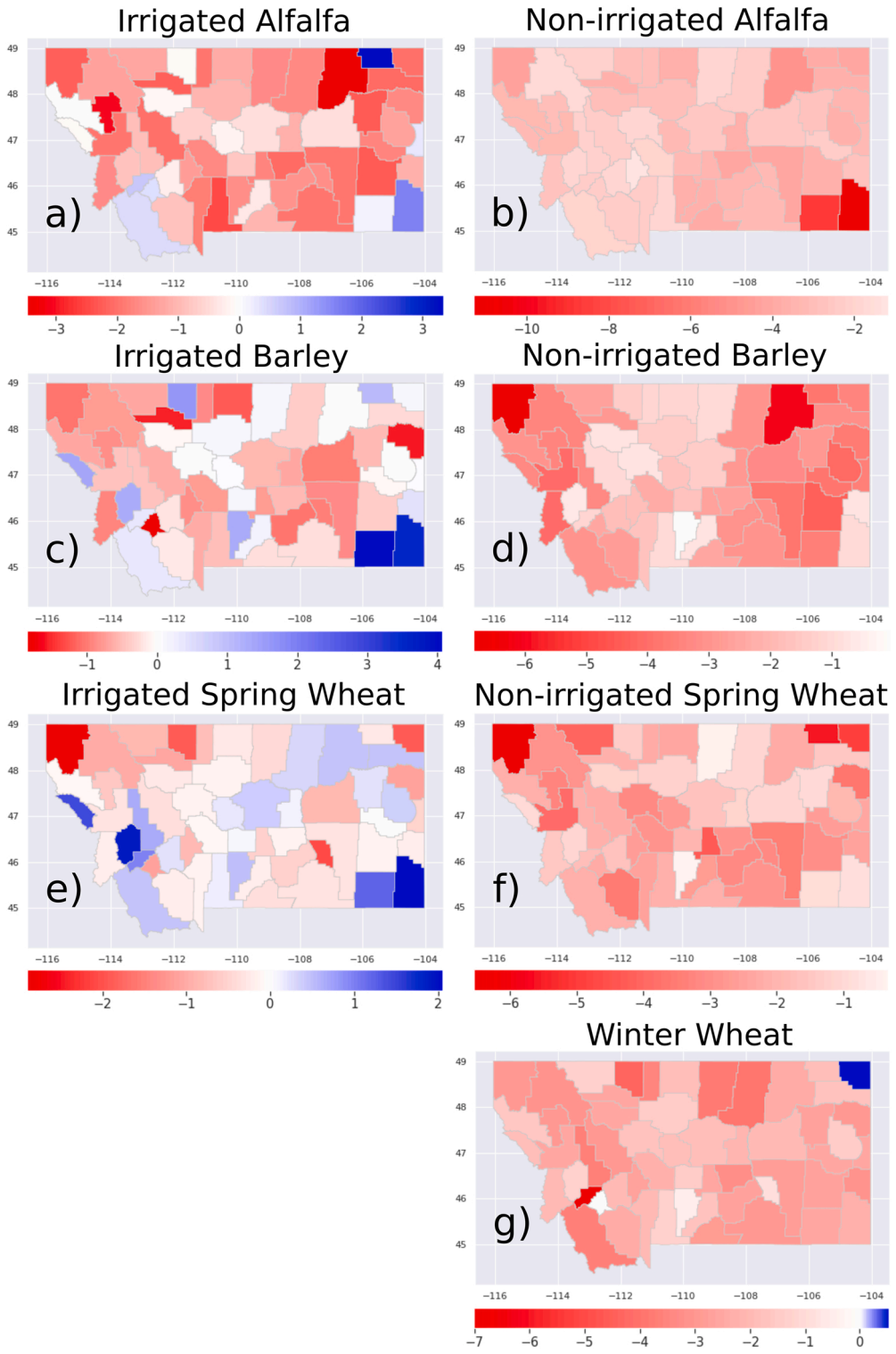

Fig. 8. County-scale median percent change (across all model climatic and economic scenarios) between the baseline (2008–2018) and end-of-century (2080–2090) projections. Different color scales for each crop type.

Table 5
Regional average values of the projected median percent changes in production for each crop type. Total range given in parentheses.

	Irrigated Alfalfa	Non-irrigated Alfalfa	Irrigated Barley	Non-irrigated Barely	Irrigated Spring Wheat	Non-irrigated Spring Wheat	Winter Wheat
Northwest	-1.1 (−3.0 to 0.7)	-2.8 (−4.3 to −1.7)	-0.2 (−1.1 to 1.4)	-3.3 (−6.8 to −0.7)	0.0 (−2.9 to 1.9)	-2.6 (−6.5 to −1.0)	-2.9 (−7.0 to −1.3)
Southwest	-0.4 (−1.8 to 0.4)	-2.1 (−2.3 to −1.8)	-0.5 (−1.9 to 0.3)	-2.3 (−2.9 to −1.6)	-0.2 (−1.1 to 0.4)	-2.4 (−3.6 to −1.6)	-2.0 (−3.6 to 0.0)
North Central	-1.2 (−2.2 to −0.1)	-2.9 (−3.7 to −1.9)	-0.3 (−1.6 to 1.6)	-1.7 (−3.0 to −0.8)	-0.6 (−1.9 to 0.3)	-1.8 (−4.1 to −0.4)	-2.8 (−4.4 to −1.3)
Central	-1.2 (−2.1 to −0.2)	-2.7 (−4.1 to −1.2)	-0.4 (−0.8 to 0.2)	-1.9 (−2.9 to −0.7)	-0.1 (−0.8 to 0.4)	-2.5 (−4.3 to −1.2)	-2.3 (−3.2 to −1.5)
South Central	-1.5 (−2.5 to −0.3)	-3.3 (−3.9 to −1.9)	-0.2 (−1.0 to 1.4)	-1.9 (−3.2 to −0.1)	-0.4 (−2.1 to 0.5)	-2.4 (−3.2 to −0.3)	-1.9 (−3.0 to −0.5)
Northeast	-1.2 (−3.5 to 3.3)	-3.6 (−4.9 to −2.5)	-0.3 (−1.6 to 1.1)	-3.8 (−6.0 to −2.9)	-0.3 (−1.9 to 0.5)	-2.7 (−5.6 to −1.0)	-1.8 (−2.9 to 0.5)
Southeast	-0.7 (−2.3 to 1.6)	-5.1 (−11.3 to −2.3)	1.0 (−0.9 to 4.1)	-3.0 (−4.4 to −0.7)	0.3 (−0.5 to 2.1)	-2.2 (−3.5 to −0.8)	-2.6 (−3.1 to −2.3)

mid-century climate change scenario. They estimated larger reductions in LU compared to our results, reductions in WU state-wide, moderate increases in crop prices, and a reduction in total gross revenues. However, their study showed that shifting to higher value crops, over less land, may translate into increased revenue per unit area in California. Likewise, farmers may choose to fallow their land and sell or lease their water to other users (Ghosh et al., 2014; Howitt et al., 2012). Montana has a limited crop portfolio and does not have a climate suitable for widespread production of high value crops that can be used to mitigate economic losses in the way California could. If in fact crop prices increase (and/or farming costs decrease), resulting in marginal land becoming economically viable, then Montana farmers may increase the extent of land area under production. Wurster et al. (2020) documented historical price anomaly impacts on crop production and showed that the majority of eastern Montana's barley production and the majority of central Montana's winter wheat production were the most sensitive to price anomalies. Therefore, shifts in market demands for barley and wheat by the end of the century could have implications for LU and WU that are not captured by our model.

5.4. Assumptions and limitations

Economic results indicated that most counties could experience PD and NR losses across all crops by the end-of-century under an RCP 8.5 carbon emissions scenario. The RCP 8.5 is increasingly considered an unrealistic scenario (Hausfather & Peters, 2020), therefore model outputs reflect the relatively extreme worst-case outcome. Our results focused on isolating the net climatic effects on agriculture; therefore, we assumed there would be no significant changes in production costs or crop market prices. Another assumption in these results was the timing of planting and irrigating. There is the potential that farmers will be able to produce more by end-of-century given warmer temperatures will allow for earlier planting dates. Crop productivity could increase with elevated CO_2 concentrations, but studies are inconclusive on the benefits of higher CO_2 when accounting for other factors, e.g., higher temperatures, disease, weather extremes (Tubiello et al., 2007). Finally, this study assumed farmers will not plant new crop types. With changing temperatures, precipitation and aridity patterns farmers may have genetically modified species, and/or begin to grow other crops, better suited for arid climates. Such crops include sorghum and pearl millet (Chipanshi et al., 2003; Jukanti et al., 2016; Silungwe et al., 2018).

In addition to the assumptions made in this study, the hydro-economic model has important limitations. First, the model did not simulate dams nor irrigation water derived from pumping groundwater. Montana's dams are important for water storage and flood mitigation and inclusion of these water storage basins could impact results in many counties. Currently, approximately 98% of Montana's water withdrawals come from surface water, therefore baseline results are deemed appropriate. On the other hand, groundwater use increases during drought periods (Taylor et al., 2013) and the severity and duration of western U.S. droughts are expected to increase (Gutzler & Robbins, 2011; Trenberth et al., 2014; Silverman et al., 2017); therefore, groundwater use for irrigation in Montana is expected to expand by the end of the century (Brown et al., 2013). However, the effects of these model limitations

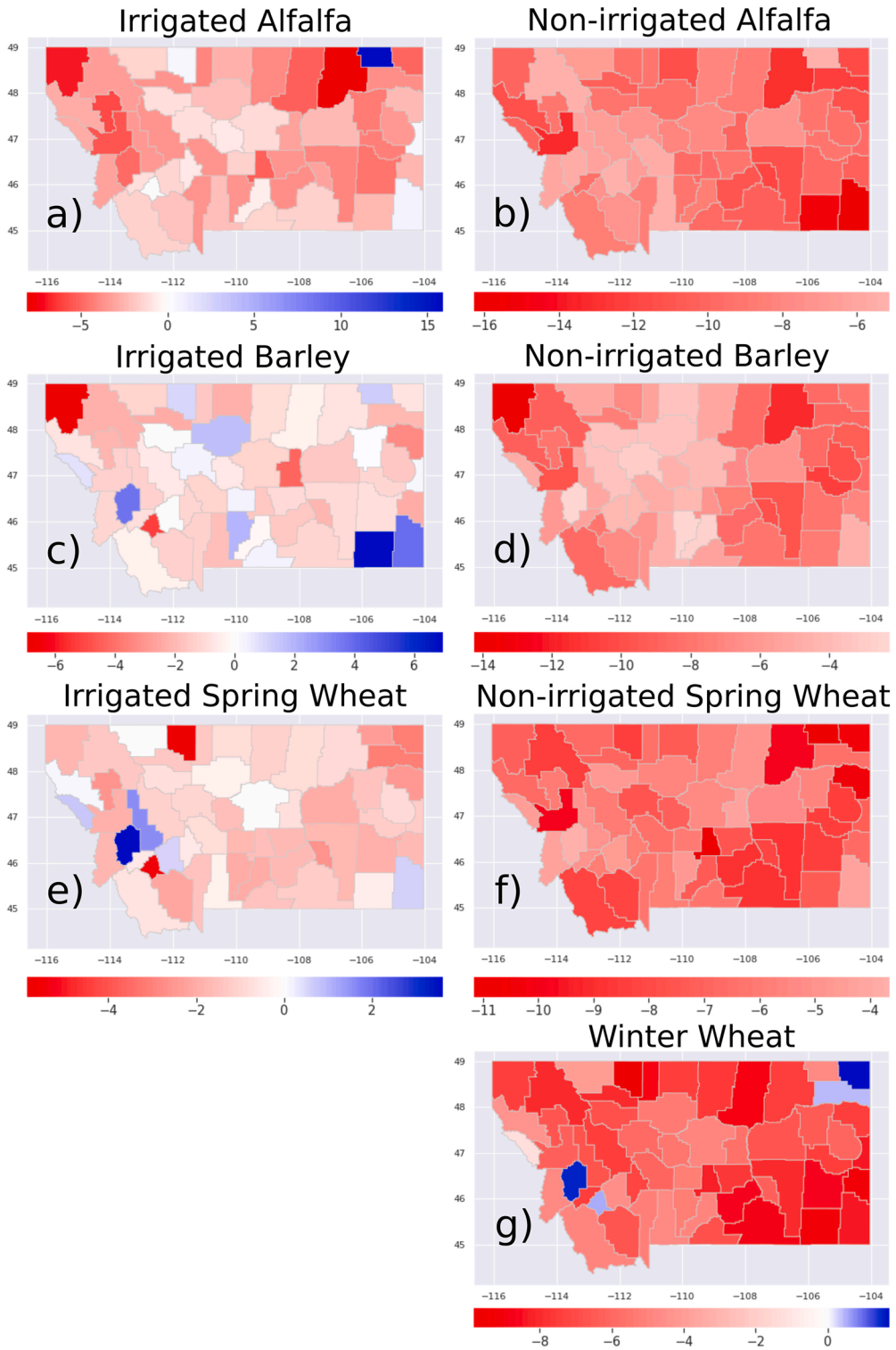

Fig. 9. County-scale median percent change (across all model climatic and economic scenarios) between the baseline (2008–2018) and end-of-century (2080–2090) projections. Different color scales for each crop type.

Table 6
Regional average values of the projected median percent changes in net revenue for each crop type. Total range given in parentheses.

	Irrigated Alfalfa	Non-irrigated Alfalfa	Irrigated Barley	Non-irrigated Barely	Irrigated Spring Wheat	Non-irrigated Spring Wheat	Winter Wheat
Northwest	-4.0 (−6.9 to −1.1)	-8.6 (−13.3 to −5.3)	-1.2 (−7.0 to 3.7)	-7.4 (−14.3 to −2.3)	-0.4 (−2.5 to 3.6)	-6.1 (−9.8 to −3.6)	-5.1 (−7.9 to 1.5)
Southwest	-1.7 (−3.6 to 0.2)	-7.3 (−8.6 to −5.1)	-1.7 (−5.2 to −0.1)	-6.7 (−8.5 to −4.1)	-1.8 (−5.5 to 0.6)	-6.6 (−8.3 to −4.6)	-4.1 (−6.7 to 0.6)
North Central	-2.6 (−5.1 to 0.6)	-9.2 (−11.3 to −6.7)	-0.7 (−2.4 to 1.7)	-5.4 (−8.5 to −3.4)	-1.4 (−5.9 to 0.0)	-6.4 (−8.4 to −4.8)	-7.5 (−9.9 to −4.1)
Central	-2.4 (−5.2 to −0.8)	-8.0 (−10.1 to −5.6)	-1.1 (−4.3 to 0.4)	-4.9 (−7.5 to −2.9)	-1.1 (−1.7 to −0.1)	-6.7 (−11.2 to −4.2)	-6.4 (−8.3 to −5.0)
South Central	-2.3 (−3.7 to −0.5)	-9.4 (−12.0 to −5.3)	-0.6 (−2.2 to 2.1)	-5.9 (−9.9 to −2.2)	-1.6 (−2.6 to −0.3)	-7.1 (−8.8 to −4.8)	-6.5 (−8.8 to −4.8)
Northeast	-1.7 (−8.2 to 15.9)	-9.9 (−13.1 to −5.2)	-1.1 (−3.4 to 1.3)	-8.9 (−11.6 to −6.3)	-2.0 (−3.1 to −0.9)	-8.4 (−11.1 to −5.2)	-4.6 (−7.5 to 1.7)
Southeast	-2.3 (−4.6 to 1.0)	-11.6 (−16.3 to −9.0)	0.8 (−2.4 to 7.0)	-8.1 (−10.7 to −4.5)	-1.1 (−1.9 to 0.6)	-7.3 (−8.9 to −4.2)	-8.4 (−9.1 to −7.5)

on the current analysis are limited because we did not use SF to estimate water available for irrigation or to calibrate the economic component. Farmer response was calibrated using water availability constraints derived from remote sensing estimates of actual crop water use during years of maximum irrigation, rather than water available in the streams (Maneta et al., 2020). In fact, SF provides a poor metric of irrigation water constraints because access to irrigation water is most often set by water regulations and not by the physical availability of water.

Regarding alfalfa production, the model optimized for NR based on market prices. Alfalfa sold on the market is valued much lower than barley or wheat. However, much of the alfalfa grown in Montana is used on-farm for cattle production, which provides a far higher value to the farmer. Since we did not incorporate the indirect revenues generated from cattle sales in the price of alfalfa, we interpreted the alfalfa market price as an opportunity cost: if a farmer chooses to use alfalfa for cattle rather than sell it on the market, then the observed price reflects a lower bound on the value of alfalfa for cattle production.

6. Conclusion

We applied an innovative, satellite-informed, integrated hydro-economic model that overcame limitations of previous studies while filling an important knowledge gap about the impacts of climate change on streamflows, land and water use, crop production, and farm net revenues. The uncertainty in climate projections and diversity of farmer adaptation responses to climate change resulted in wide uncertainty in predicted states of streamflow, agricultural water use, and net revenues. By the end of the century, the majority of rivers across Montana would experience streamflow declines of 10–30% during the summer months. Our simulations showed a state-wide increase of 1.6% in land area devoted to irrigated crops accompanied by an 18.2% increase in agricultural water use. Montana is the headwaters to three major watersheds; therefore, declines in growing season water availability and increases in agricultural water demand would have far reaching impacts downstream. Even accounting for the increases in irrigated land and water use, irrigated crop production and farm net revenues were expected to decline by 0.5% and 1.5%, respectively. Projections for rainfed crops were more dire. Collectively, state-wide land allocated to rainfed crops declined 6.5%, production declined 2.7%, and net revenue declined 7.2%. While our study simulated the hydro-economic impacts of climate change in Montana, our results are representative of what many regions in the Intermountain West would experience. Our study filled important knowledge gaps by incorporating a wide range of economic and climate variability that are reflected in a comprehensive range of future predictions.

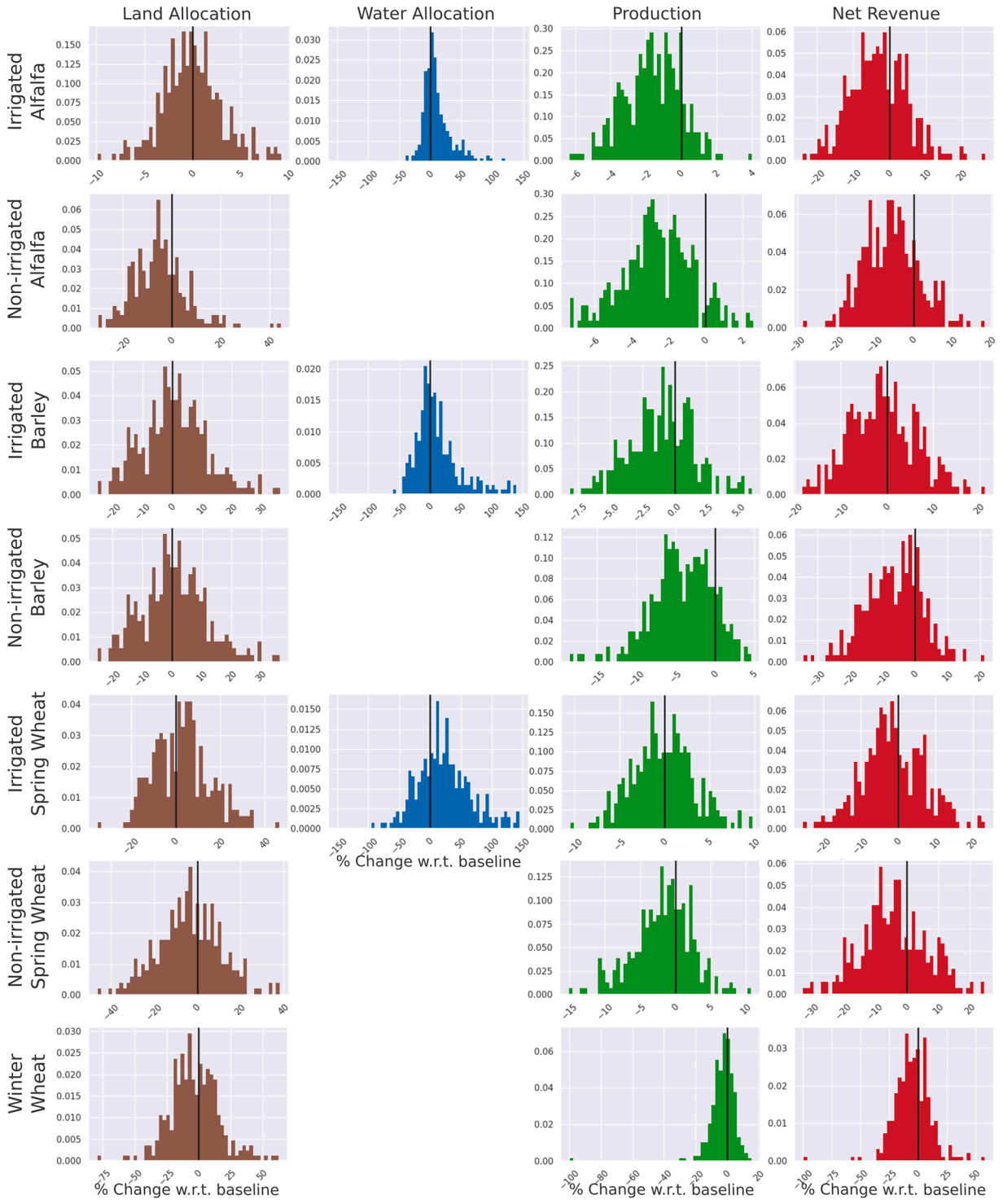

Fig. 10. Probability distributions of economic model results (columns) for each crop type (rows) for Ravalli County. Refer to Fig. 1b for county location and Fig. 4b for hydrologic model results.

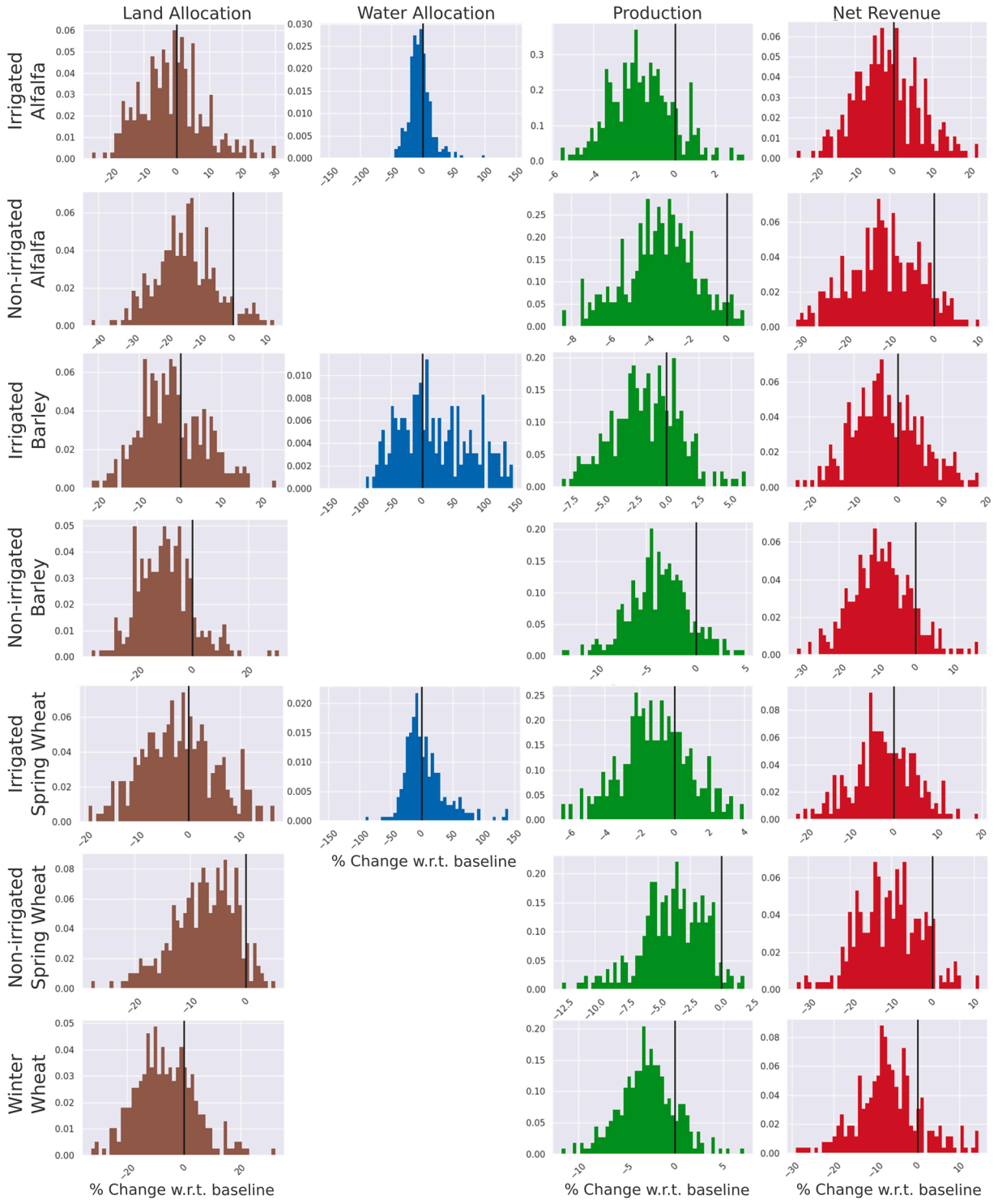

Fig. 11. Probability distributions of economic model results (columns) for each crop type (rows) for Richland County. Refer to Fig. 1b for county location and Fig. 4c for hydrologic model results.

CRediT authorship contribution statement

The authors declare that they have no known competing financial interests or personal relationships that could have appeared to influence the work reported in this paper.

Declaration of Competing Interest

The authors declare that they have no known competing financial interests or personal relationships that could have appeared to influence the work reported in this paper.

Acknowledgments

This work was conducted at the University of Montana with support from the following grants: USDA-NIFA [2016–67026-25067], NASA EPSCoR [80NSSC18M0025], and MITRE Cropland Climate [1160380]. Zachary H. Lauffenburger acknowledges support from the University of Montana BRIDGES program through funding from the National Science Foundation [DGE-1633831, OIA-1920938 and OIA-1738857]; and the Montana Water Center through funding from the USGS 104b Water Resources Research program.

Appendix A. Hydrologic component

The HBV model conceptualizes each sub-catchment delineated in Fig. 1a as a cascade of four compartments that represent water storages (Fig. A1) (Wallner et al., 2013). Daily water outputs from the soil and two groundwater compartments are transformed into runoff to the stream using a convolution with a triangular unit hydrograph (Soil Conservation Service, 1972). Runoff is then routed through the stream network using the Muskingum-Cunge method of river routing (Cunge, 1969). The Muskingum-Cunge method is a water routing model that enforces the conservation of mass at each node of the river network. See technical appendices in Maneta et al. (2020) for a detailed description of the hydrologic component.

Appendix B. Economic component

The objective function for the economic component is as follows:

$$max_{x_{land,i},x_{water,i}} net = \sum_i \left\{ p_i \pi_i \left(x_{land,i}, x_{water,i}; \mu_i, \quad \beta_{land,i}, \quad \beta_{water,i}, \quad \rho_i, \quad \delta_i \right) - \quad c_{land,i} x_{land,i} - c_{water,i} x_{water,i} \right\}$$

Subject to:

$$\sum_i x_{land,i} \leq \overline{L}$$

$$\sum_i x_{water,i} \leq \overline{W}$$

$$x_{land,i} = \quad \overline{x}_{land,i} \quad [\lambda_{land,i}]$$

$$x_{water,i} = \quad \overline{x}_{water,i} \quad [\lambda_{water,i}]$$

$$x_{land,i}, x_{water,i} \geq 0 \tag{B1}$$

where *net* is the net revenue, defined as revenue less the cost of land and water use; the index $i = 1, \ldots, I$ represent crops; $x_{land,i}$, $x_{water,i}$ represent land and water resource inputs for crop i, respectively; $_{pi}$ is the price received for crop i; π_i is the production function that associates resource inputs to total production of crop i; and $c_{land,i}$, $c_{water,i}$ are the unit costs associated with land and water use to produce crop i. The parameters μ, β, ρ, δ are production function parameters (described below). The constraints in Eq. (B1) require that the total land and water used for all crops in the region is less than or equal to the total land $\overline{L}$ and water $\overline{W}$ available for cultivation, as well as standard non-negativity constraints. The Lagrange multiplier parameters, $\lambda_{land,i}$ and $\lambda_{water,i}$, associated with the observed land and water-use constraints, respectively, represent the shadow prices of land and water.

$$\pi_i = \mu_i \left[\beta_{land,i} x_{land,i}^{\rho_i} + \beta_{water,i} \left(x_{water,i} + x_{precip,i} \right)^{\rho_i} \right]^{\frac{\delta_i}{\rho_i}} \tag{B2}$$

where μ, β, ρ, δ represent the production factor, share parameter, elasticity of substitution and return-to-scale parameter, respectively. The PMP methodology finds the production and cost function parameters that maximize Eq. (B1) while the values of land and water allocation are fixed to observed levels. The PMP methodology results in a calibrated function that captures observed producer behavior under the assumption that producers allocate resources to maximize net revenues subject to resource constraints (Howitt, 1995). Information on supply elasticity and yield elasticity is taken into account during the calibration following Mérel et al. (2011) and Garnache et al. (2017). The model captures producer response to crop prices and the geographical sensitivity of crop production to

water applications. The model also adjusts the cost of land and water in geographical space from county-level observations of land and water allocations via the calibrated shadow values.

We specify daily water diversion rates from source node j in the stream network, and for each crop i, by redistributing the mean of the modeled probability distribution of seasonal water allocation [$x_{water,i}$] into daily amounts over the growing season according to a fractional weight coefficient $\omega_{i,t+1}$ that reflects the growth stage of the crop at a given day:

$$q^{irr}_{j,i,t+1} = \frac{\mathbb{E}[x_{water,i}] * \omega_{i,t+1}}{I_{eff_i}} \tag{B3}$$

where:

$$\omega_{i,t+1} = \frac{Kc_{i,t+1}}{\sum_i Kc_{i,t+1}} \tag{B4}$$

where $q^{irr}_{j,i,t+1}$ is the water volume diverted for irrigation from stream node j for crop i at day $t+1$; $\mathbb{E}[x_{water,i}]$ is the expectation of the ensemble of water allocations produced by the economic component of the model; I_{eff_i} is an irrigation and conveyance efficiency factor for crop i; and $\omega_{i,t+1}$ is a weight factor that represents the fraction of the total crop water requirement that corresponds to day $t+1$ and is a function of crop coefficients Kc_{t+1} that vary through the season from plant emergence to full cover to termination. Kc reflects the crop evapotranspiration at a given growth stage with respect to evapotranspiration of a fully developed reference crop (alfalfa). We obtained crop coefficients and growth curves for each crop from the U.S. Bureau of Reclamation (USBR) for the Pacific Northwest Region AgriMet program (USBR, 2016).

Appendix C. Economic model data sources

Refer to Maneta et al. (2020) for a comprehensive description of the economic model. Data on annual variations of crop type mosaic and land area in crops over each economic unit (county) were obtained from the USDA Cropland Data Layer, which provides satellite-based remote sensing crop-specific land cover classification at a 30 m spatial resolution (USDA NASS, 2015). Crop production was calculated using a satellite-driven light use efficiency model to estimate gross primary production at a 30 m resolution and 8-day time step (He et al., 2018), and then aggregated to produce county-scale total production. Total water used by each crop (CWU_{base}), which includes both evapotranspiration from precipitation and from supplemental irrigation, was estimated at 30 m spatial resolution and 8-day temporal frequency by adapting the operational NASA MOD16A2 global evapotranspiration product (Mu et al., 2011) for agricultural applications (He et al., 2019). County-scale CWU_{base} volumes were obtained by accumulating pixel-scale, 8-day evapotranspiration estimates over the growing season (April 1st – September 30th). Uncertainty in CWU_{base} was obtained by scaling the spatial standard deviation of crop evapotranspiration by the area planted. Planting and harvesting dates vary year to year based on many factors, most notably field and crop conditions. The growing season date range we used was chosen to be inclusive of the usual planting and harvesting dates reported in USDA NASS (2010), and because irrigation water rights in Montana start April 1st (MT DNRC, 2017). Crop price data and the approximated costs of cultivating land and applying water were obtained from USDA NASS at the state-scale. Irrigation-system efficiencies for each economic unit were calculated using the Food and Agriculture Organization of the United Nations (FAO) scheme irrigation efficiency equation (Brouwer et al., 1989). Irrigation method (flood or sprinkler) statistics were obtained from the Montana Water Rights Database (MT DNRC, 2017).

Appendix D. Supporting information

Supplementary data associated with this article can be found in the online version at doi:10.1016/j.ejrh.2022.101127.

References

Abatzoglou, J.T., 2013. Development of gridded surface meteorological data for ecological applications and modelling. Int. J. Climatol. 33 (1), 121–131. https://doi.org/10.1002/joc.3413.

Anderson, B., 2016. Heat Effects on Alfalfa. Institute of Agriculture and Natural Resources. University of Nebraska - Lincoln, accessed 13 April 2020. https://cropwatch.unl.edu/2016/heat-effects-alfalfa.

Anderson, M.B., Ward, L.C., Gilbertz, S.J., McEvoy, J., Hall, D.M., 2018. Prior appropriation and water planning reform in Montana's Yellowstone River Basin: path dependency or boundary object? J. Environ. Pol. Plann. 20 (2), 198–213. https://doi.org/10.1080/1523908X.2017.1348286.

Asseng, S., Ewert, F., Rosenzweig, C., Jones, J.W., Hatfield, J.L., Ruane, A.C., et al., 2013. Uncertainty in simulating wheat yields under climate change. Nat. Climate Change 3 (9), 827–832. https://doi.org/10.1038/nclimate1916.

Averyt, K., Meldrum, J., Caldwell, P., Sun, G., McNulty, S., Huber-Lee, A., Madden, N., 2013. Sectoral contributions to surface water stress in the coterminous United States. Environ. Res. Lett. 8 (3), 035046 https://doi.org/10.1088/1748-9326/8/3/035046.

Bales, R.C., Molotch, N.P., Painter, T.H., Dettinger, M.D., Rice, R., Dozier, J., 2006. Mountain hydrology of the western United States. Water Resour. Res. 42 (8), W08432. https://doi.org/10.1029/2005WR004387.

Bergström, S., Forsman, A., 1973. Development of a conceptual deterministic Rainfall-Runoff model. Nordic Hydrol. 4 (3), 147–170. https://doi.org/10.2166/nh.1973.0012.

Bergström, S. (1995). The HBV model. In Singh, V.P. , & Woolhiser, D.A., 2002, Mathematical Modeling of Watershed Hydrology. Journal of Hydrologic Engineering 7 (4), 270–292. https://doi.org/10.1061/(ASCE)1084–0699(2002)7:4(270).

Borrego-Marín, M.M., Expoísito, A., Berbel, J., 2020. A simplified hydro-economic model of guadalquivir river basin for analysis of water-pricing scenarios. Water ((Switzerland)) 12 (7), 1879. https://doi.org/10.3390/W12071879.
Brouwer, C., Prins, K., Heilbloem, M., 1989. Irrigation Water Management: Irrigation Scheduling, Training manual No. 4. FAO,, Rome, Italy.
Brouwer, R., Hofkes, M., 2008. Integrated hydro-economic modelling: Approaches, key issues and future research directions. Ecol. Econ. 66 (1), 16–22. https://doi.org/10.1016/j.ecolecon.2008.02.009.
Brown, T.C., Foti, R., Ramirez, J.A., 2013. Projected freshwater withdrawals in the United States under a changing climate. Water Resour. Res. 49 (3), 1259–1276. https://doi.org/10.1002/wrcr.20076.
Chipanshi, A.C., Chanda, R., Totolo, O., 2003. Vulnerability assessment of the maize and sorghum crops to climate change in Botswana. Climatic Change 61 (3), 339–360. https://doi.org/10.1023/B:CLIM.0000004551.55871.eb.
Colligan, T., Ketchum, D., Brinkerhoff, D., Maneta, M., 2021. A Deep Learning Approach to Mapping Irrigation: IrrMapper-U-Net. arXiv Prepr. arXiv2 103, 03278.
Connell-Buck, C.R., Medellín-Azuara, J., Lund, J.R., Madani, K., 2011. Adapting California's water system to warm vs. dry climates. Climatic Change 109, 133–149. https://doi.org/10.1007/s10584-011-0302-7.
Cross, W.F., LaFave, J., Leone, A., Lonsdale, W., Royem, A., Patton, T., McGinnis, S., 2017. Chapter 3: water and climate change in Montana. In: Whitlock, C., Cross, W., Maxwell, B., Silverman, N., Wade, A. (Eds.), (. Montana Institute on Ecosystems, pp. 79–148. https://doi.org/10.15788/M2WW8W.
Cunge, J.A., 1969. On the subject of a flood propagation computation method (musklngum method). J. Hydraulic Res. 7 (2), 205–230. https://doi.org/10.1080/00221686909500264.
Das, T., Pierce, D.W., Cayan, D.R., Vano, J.A., Lettenmaier, D.P., 2011. The importance of warm season warming to western U.S. streamflow changes. Geophys. Res. Lett. 38 (23), L23403. https://doi.org/10.1029/2011GL049660.
Döll, P., 2002. Impact of climate change and variability on irrigation requirements: A global perspective. Climatic Change 54 (3), 269–293. https://doi.org/10.1023/A:1016124032231.
Edwards, E.C., Smith, S.M., 2018. The role of irrigation in the development of agriculture in the United States. J. Econ. Hist. 78 (4), 1103–1141. https://doi.org/10.1017/S0022050718000608.
Esteve, P., Varela-Ortega, C., Blanco-Gutiérrez, I., Downing, T.E., 2015. A hydro-economic model for the assessment of climate change impacts and adaptation in irrigated agriculture. Ecol. Econ. 120, 49–58. https://doi.org/10.1016/j.ecolecon.2015.09.017.
Falloon, P., Betts, R., 2010. Climate impacts on European agriculture and water management in the context of adaptation and mitigation-The importance of an integrated approach. Sci. Total Environ. 408 (23), 5667–5687. https://doi.org/10.1016/j.scitotenv.2009.05.002.
Ficklin, D.L., Stewart, I.T., Maurer, E.P., 2013. Climate change impacts on streamflow and subbasin-scale hydrology in the Upper Colorado River Basin. PloS One 8 (8), e71297. https://doi.org/10.1371/journal.pone.0071297.
Ficklin, D.L., Novick, K.A., 2017. Historic and projected changes in vapor pressure deficit suggest a continental-scale drying of the United States atmosphere. J. Geophys. Res.: Atmos. 122 (4), 2061–2079. https://doi.org/10.1002/2016JD025855.
Fischer, G., Tubiello, F.N., van Velthuizen, H., Wiberg, D.A., 2007. Climate change impacts on irrigation water requirements: Effects of mitigation, 1990-2080. Technol. Forecast. Social Change 74 (7), 1083–1107. https://doi.org/10.1016/j.techfore.2006.05.021.
Fu, Q., Feng, S., 2014. Responses of terrestrial aridity to global warming. J. Geophys. Res. 119 (13), 7863–7875. https://doi.org/10.1002/2014JD021608.
Garnache, C., Mérel, P., Howitt, R., Lee, J., 2017. Calibration of shadow values in constrained optimisation models of agricultural supply. Eur. Rev. Agricult. Econ. 44 (3), 363–397. https://doi.org/10.1093/erae/jbx005.
Ghosh, S., Cobourn, K.M., Elbakidze, L., 2014. Water banking, conjunctive administration, and drought: The interaction of water markets and prior appropriation in Southeastern Idaho. Water Resour. Res. 50 (8), 6927–6949. https://doi.org/10.1002/2014WR015572.
Grantham, T.E., Viers, J.H., 2014. 100 years of California's water rights system: Patterns, trends and uncertainty. Environ. Res. Lett. 9 (8), 84012. https://doi.org/10.1088/1748-9326/9/8/084012.
Greve, P., Roderick, M.L., Ukkola, A.M., Wada, Y., 2019. The aridity Index under global warming. Environ. Res. Lett. 14 (12), 124006 https://doi.org/10.1088/1748-9326/ab5046.
Groves, D.G., Yates, D., Tebaldi, C., 2008. Developing and applying uncertain global climate change projections for regional water management planning. Water Resour. Res. 44 (12), W12413. https://doi.org/10.1029/2008WR006964.
Gupta, H. v, Kling, H., Yilmaz, K.K., Martinez, G.F., 2009. Decomposition of the mean squared error and NSE performance criteria: Implications for improving hydrological modelling. J. Hydrol. 377 (1–2), 80–91. https://doi.org/10.1016/j.jhydrol.2009.08.003.
Gutzler, D.S., Robbins, T.O., 2011. Climate variability and projected change in the western United States: Regional downscaling and drought statistics. Climate Dyn. 37 (5), 835–849. https://doi.org/10.1007/s00382-010-0838-7.
Hanjra, M.A., Ferede, T., Gutta, D.G., 2009. Reducing poverty in sub-Saharan Africa through investments in water and other priorities. Agricult. Water Manag. 96 (7), 1062–1070. https://doi.org/10.1016/j.agwat.2009.03.001.
Harou, J.J., Pulido-Velazquez, M., Rosenberg, D.E., Medellín-Azuara, J., Lund, J.R., Howitt, R.E., 2009. Hydro-economic models: Concepts, design, applications, and future prospects. J. Hydrol. 375 (3–4), 627–643. https://doi.org/10.1016/j.jhydrol.2009.06.037.
Hartigan, J.A., Wong, M.A., 1979. Algorithm AS 136: A K-Means Clustering Algorithm. Appl. Stat. 28 (1), 100. https://doi.org/10.2307/2346830.
Hausfather, Z., Peters, G.P., 2020. Emissions – the 'business as usual' story is misleading. Nature 577 (7792), 618–620. https://doi.org/10.1038/d41586-020-00177-3.
He, M., Kimball, J.S., Maneta, M.P., Maxwell, B.D., Moreno, A., Beguería, S., Wu, X., 2018. Regional crop gross primary productivity and yield estimation using fused landsat-MODIS data. Remote Sens. 10 (3), 372. https://doi.org/10.3390/rs10030372.
He, M., Kimball, J.S., Yi, Y., Running, S.W., Guan, K., Moreno, A., Wu, X., Maneta, M., 2019. Satellite data-driven modeling of field scale evapotranspiration in croplands using the MOD16 algorithm framework. Remote Sens. Environ. 230, 111201 https://doi.org/10.1016/j.rse.2019.05.020.
Howitt, R.E., 1995. Positive mathematical programming. Am. J. Agricult. Econ. 77 (2), 329–342. https://doi.org/10.2307/1243543.
Howitt, R.E., Medellín-Azuara, J., MacEwan, D., Lund, J.R., 2012. Calibrating disaggregate economic models of agricultural production and water management. Environ. Modell. Softw. 38, 244–258. https://doi.org/10.1016/j.envsoft.2012.06.013.
Jukanti, A.K., Gowda, C.L., Rai, K.N., Manga, V.K., Bhatt, R.K., 2016. Crops that feed the world 11. Pearl Millet (Pennisetum glaucum L.): an important source of food security, nutrition and health in the arid and semi-arid tropics. Food Sec. 8 (2), 307–329. https://doi.org/10.1007/s12571-016-0557-y.
Ketchum, D., Jencso, K., Maneta, M.P., Melton, F., Jones, M.O., Huntington, J., 2020. IrrMapper: A Machine Learning Approach for High Resolution Mapping of Irrigated Agriculture Across the Western US. Remote Sens. 12 (14), 2328. https://doi.org/10.3390/rs12142328.
Kim, Y., Kimball, J.S., Didan, K., Henebry, G.M., 2014. Response of vegetation growth and productivity to spring climate indicators in the conterminous United States derived from satellite remote sensing data fusion. Agricult. For. Meteorol. 194, 132–143. https://doi.org/10.1016/j.agrformet.2014.04.001.
Lanning, S.P., Kephart, K., Carlson, G.R., Eckhoff, J.E., Stougaard, R.N., Wichman, D.M., et al., 2010. Climatic change and agronomic performance of hard red spring wheat from 1950 to 2007. Crop Sci. 50 (3), 835–841. https://doi.org/10.2135/cropsci2009.06.0314.
Lauffenburger, Z.H., Gurdak, J.J., Hobza, C., Woodward, D., Wolf, C., 2018. Irrigated agriculture and future climate change effects on groundwater recharge, northern High Plains aquifer, USA. Agricult. Water Manag. 204, 69–80. https://doi.org/10.1016/j.agwat.2018.03.022.
Li, D., Wrzesien, M.L., Durand, M., Adam, J., Lettenmaier, D.P., 2017. How much runoff originates as snow in the western United States, and how will that change in the future? Geophys. Res. Lett. 44 (12), 6163–6172. https://doi.org/10.1002/2017GL073551.
Lindström, G., Johansson, B., Persson, M., Gardelin, M., Bergström, S., 1997. Development and test of the distributed HBV-96 hydrological model. J. Hydrol. 201 (1–4), 272–288. https://doi.org/10.1016/S0022-1694(97)00041-3.
Maneta, M.P., Torres, M.O., Wallender, W.W., Vosti, S., Howitt, R., Rodrigues, L., et al., 2009. A spatially distributed hydroeconomic model to assess the effects of drought on land use, farm profits, and agricultural employment. Water Resour. Res. 45 (11), W11412. https://doi.org/10.1029/2008WR007534.
Maneta, M.P., Cobourn, K., Kimball, J.S., He, M., Silverman, N.L., Chaffin, B.C., et al., 2020. A satellite-driven hydro-economic model to support agricultural water resources management. Environ. Model. Softw. 134, 104836 https://doi.org/10.1016/j.envsoft.2020.104836.

Maxwell, B., Weed, B., Ippolito, L., Bekkerman, A., Boone, M., Mills-Novoa, M., et al., 2017. Chapter 5: Agriculture and Climate Change in Montana. In: Whitlock, C., Cross, W., Maxwell, B., Silverman, N., Wade, A. (Eds.), (. Montana Institute on Ecosystems, pp. 197–244. https://doi.org/10.15788/M2WW8W.
McCabe, G.J., Clark, M.P., 2005. Trends and variability in snowmelt runoff in the western United States. J. Hydrometeorol. 6 (4), 476–482. https://doi.org/10.1175/JHM428.1.
Medellín-Azuara, J., Howitt, R.E., MacEwan, D.J., Lund, J.R., 2011. Economic impacts of climate-related changes to California agriculture. Climatic Change 109, 387–405. https://doi.org/10.1007/s10584-011-0314-3.
Mérel, P., Simon, L.K., Yi, F., 2011. A fully calibrated generalized constant-elasticity-of-substitution programming model of agricultural supply. Am. J. Agricult. Econ. 93 (4), 936–948. https://doi.org/10.1093/ajae/aar029.
MT DNRC, Montana Department of Natural Resources and Conservation, 2014. Montana State Water Plan 2015—a Watershed Approach. Helena, Montana,, p. 84. http://dnrc.mt.gov/divisions/water/management/docs/state-water-plan/2015_mt_water_plan.pdf.
MT DNRC, Montana Department of Natural Resources and Conservation, 2017. Water Resources Division, Montana Water Rights. Helena, MT: Montana State Library,. http://ftp.geoinfo.msl.mt.gov/Data/Spatial/NonMSDI/DNRC_WR/.
Mu, Q., Zhao, M., Running, S.W., 2011. Improvements to a MODIS global terrestrial evapotranspiration algorithm. Remote Sens. Environ. 115 (8), 1781–1800. https://doi.org/10.1016/j.rse.2011.02.019.
Paltasingh, K.R., Goyari, P., Mishra, R.K., 2012. Measuring weather impacts on crop yield using aridity index. Indian Agricult. Econ. Res. Rev. 25 (2), 205–216 accessed 18 December 2019. https://ageconsearch.umn.edu/record/137373/.
Pathak, T.B., Maskey, M.L., Dahlberg, J.A., Kearns, F., Bali, K.M., Zaccaria, D., 2018. Climate change trends and impacts on California Agriculture: A detailed review. Agronomy 8 (3), 25. https://doi.org/10.3390/agronomy8030025.
Pederson, G.T., Gray, S.T., Ault, T., Marsh, W., Fagre, D.B., Bunn, A.G., et al., 2011. Climatic controls on the snowmelt hydrology of the northern Rocky Mountains. J. Climate 24 (6), 1666–1687. https://doi.org/10.1175/2010JCLI3729.1.
Rauscher, S.A., Pal, J.S., Diffenbaugh, N.S., Benedetti, M.M., 2008. Future changes in snowmelt-driven runoff timing over the western US. Geophys. Res. Lett. 35 (16), L16703. https://doi.org/10.1029/2008GL034424.
Regonda, S.K., Rajagopalan, B., Clark, M., Pitlick, J., 2005. Seasonal cycle shifts in hydroclimatology over the western United States. J. Climate 18 (2), 372–384. https://doi.org/10.1175/JCLI-3272.1.
Roderick, M.L., Greve, P., Farquhar, G.D., 2015. On the assessment of aridity with changes in atmospheric CO_2. Water Resour. Res. 51 (7), 5450–5463. https://doi.org/10.1002/2015WR017031.
Rousseeuw, P.J., 1987. Silhouettes: A graphical aid to the interpretation and validation of cluster analysis. J. Comput. Appl. Math. 20 (C), 53–65. https://doi.org/10.1016/0377-0427(87)90125-7.
Rupp, D.E., Abatzoglou, J.T., Hegewisch, K.C., Mote, P.W., 2013. Evaluation of CMIP5 20th century climate simulations for the Pacific Northwest USA. J. Geophys. Res. Atmos. 118 (19), 10,884–10,906. https://doi.org/10.1002/jgrd.50843.
Schaible, G.D., Kim, C.S., Aillery, M.P., 2010. Dynamic Adjustment of Irrigation Technology/Water Management in Western U.S. Agriculture: Toward a Sustainable Future. Can. J. Agricult. Econ. 58 (4), 433–461. https://doi.org/10.1111/j.1744-7976.2010.01199.x.
Schauberger, B., Archontoulis, S., Arneth, A., Balkovic, J., Ciais, P., Deryng, D., et al., 2017. Consistent negative response of US crops to high temperatures in observations and crop models. Nat. Commun. 8, 1–9. https://doi.org/10.1038/ncomms13931.
Scheff, J., Frierson, D.M.W., 2015. Terrestrial aridity and its response to greenhouse warming across CMIP5 climate models. J. Climate 28 (14), 5583–5600. https://doi.org/10.1175/JCLI-D-14-00480.1.
Sherwood, S., Fu, Q., 2014. A drier future? Science 343 (6172), 737–739. https://doi.org/10.1126/science.1247620.
Siderius, C., van Walsum, P.E.V., Roest, C.W.J., Smit, A.A.M.F.R., Hellegers, P.J.G.J., Kabat, P., van Ierland, E.C., 2016. The role of rainfed agriculture in securing food production in the Nile Basin. Environ. Sci. Policy 61, 14–23. https://doi.org/10.1016/j.envsci.2016.03.007.
Silungwe, F.R., Graef, F., Bellingrath-Kimura, S.D., Tumbo, S.D., Kahimba, F.C., Lana, M.A., 2018. crop upgrading strategies and modelling for rainfed cereals in a semi-arid climate-A review. Water ((Switzerland)) 10 (4), 356. https://doi.org/10.3390/w10040356.
Silverman, N., Jencso, K., Herendeen, P., Royem, A., Sweet, M., Brust, B., 2017. Chapter 2: Climate Change in Montana. In: Whitlock, C., Cross, W., Maxwell, B., Silverman, N., Wade, A. (Eds.), (. Montana Institute on Ecosystems, pp. 9–70. https://doi.org/10.15788/M2WW8W.
Slaughter, R.A., Hamlet, A.F., Huppert, D., Hamilton, J., Mote, P.W., 2010. Mandates vs markets: Addressing over-allocation of Pacific Northwest River Basins. Water Policy 12 (3), 305–317. https://doi.org/10.2166/wp.2009.152.
Soil Conservation Service, 1972. National Engineering Handbook. Section 4, U.S. Department of Agriculture,, Washington, D.C.
Soil Survey Staff, Natural Resources Conservation Service, United States Department of Agriculture. Soil Survey Geographic (SSURGO) Database. ⟨https://sdmdataaccess.sc.egov.usda.gov⟩ (accessed 1 December 2018).
Tack, J., Barkley, A., Hendricks, N., 2017. Irrigation offsets wheat yield reductions from warming temperatures. Environ. Res. Lett. 12 (11), 114027 https://doi.org/10.1088/1748-9326/aa8d27.
Tanaka, S.K., Zhu, T., Lund, J.R., Howitt, R.E., Jenkins, M.W., Pulido, M.A., Tauber, M., Ritzema, R.S., Ferreira, I.C., 2006. Climate warming and water management adaptation for California. Climatic Change 76 (3–4), 361–387. https://doi.org/10.1007/s10584-006-9079-5.
Taylor, R.G., Scanlon, B., Döll, P., Rodell, M., van Beek, R., Wada, Y., et al., 2013. Ground water and climate change. Nat. Climate Change 3 (4), 322–329. https://doi.org/10.1038/nclimate1744.
Torres, M.D.O., Maneta, M., Howitt, R., Vosti, S.A., Wallender, W.W., Bassoi, L.H., Rodrigues, L.N., 2012. Economic impacts of regional water scarcity in the São Francisco river Basin, Brazil: An application of a linked hydro-economic model. Environ. Dev. Econ. 17 (2), 227–248. https://doi.org/10.1017/S1355770×11000362.
Trenberth, K.E., Dai, A., van der Schrier, G., Jones, P.D., Barichivich, J., Briffa, K.R., Sheffield, J., 2014. Global warming and changes in drought. Nat. Climate Change 4 (1), 17–22. https://doi.org/10.1038/nclimate2067.
Tubiello, F.N., Soussana, J.F., Howden, S.M., 2007. Crop and pasture response to climate change. Proc. Natl. Acad. Sci. U. S. A. 104 (50), 19686–19690. https://doi.org/10.1073/pnas.0701728104.
Udall, B., Overpeck, J., 2017. The twenty-first century Colorado River hot drought and implications for the future. Water Resour. Res. 53 (3), 2404–2418. https://doi.org/10.1002/2016WR019638.
U.S. Bureau of Reclamation, 2016, AgriMet Crop Coefficients. ⟨https://www.usbr.gov/pn/agrimet/cropcurves/crop_curves.html⟩ (accessed 1 September 2018).
[USDA NASS] U.S. Department of Agriculture National Agricultural Statistics Service, 2010, Field crops: Usual planting and harvesting dates. USDA National Agricultural Statistics Service, Agricultural Handbook, 628. ⟨https://www.nass.usda.gov/Publications/Todays_Reports/reports/fcdate10.pdf⟩ (accessed 11 February 2021).
[USDA NASS] U.S. Department of Agriculture National Agricultural Statistics Service, 2015, Cropland data layer. Published crop-specific data layer [Online], USDA-NASS. Washington, DC. ⟨https://nassgeodata.gmu.edu/CropScape/⟩ (accessed 1 September 2018).
[USDA NASS] U.S. Department of Agriculture National Agricultural Statistics Service, 2017, Census of Agriculture. ⟨www.nass.usda.gov/AgCensus⟩ (accessed 4 October 2020).
[USGS] U.S. Geological Survey, 1996, USGS EROS Archive – Digital Elevation – Global 30 Arc-Second Elevation (GTOPO30). ⟨https://doi.org/10.5066/F7DF6PQS⟩.
[USGS] U.S. Geological Survey, 2018, Water Use in Montana. ⟨https://www.usgs.gov/centers/wy-mt-water/science/water-use-montana?qt-science_center_objects=0#qt-science_center_objects⟩ (accessed 1 December 2019).
U.S. Global Change Research Program, 2017. In: Wuebbles, D.J., Fahey, D.W., Hibbard, K.A., Dokken, D.J., Stewart, B.C., Maycock, T.K. (Eds.), Climate Science Special Report: Fourth National Climate Assessment, Volume I. U.S. Global Change Research Program, Washington, DC, USA, p. 470. ⟨https://doi.org/10.7930/J0J964J6⟩.
Wallner, M., Haberlandt, U., Dietrich, J., 2013. A one-step similarity approach for the regionalization of hydrological model parameters based on self-organizing maps. J. Hydrol. 494, 59–71. https://doi.org/10.1016/j.jhydrol.2013.04.022.

Walter, I.A., Allen, R.G., Elliott, R., Jensen, M.E., Itenfisu Mecham, D., et al., 2000. ASCE's standardized reference evapotranspiration equation. Watershed Manag. Operations Manag. 2000 105, 1–11. ⟨https://doi.org/10.1061/40499⟩(2000)126.

Ward, F.A., Booker, J.F., Michelsen, A.M., 2006. Integrated Economic, Hydrologic, and Institutional Analysis of Policy Responses to Mitigate Drought Impacts in Rio Grande Basin. J. Water Resour. Plann. Manag. 132 (6), 488–502. https://doi.org/10.1061/(asce)0733-9496(2006)132:6(488).

Warrick, A.W., Gardner, W.R., 1983. Crop yield as affected by spatial variations of soil and irrigation. Water Resour. Res. 19 (1), 181–186. https://doi.org/10.1029/WR019i001p00181.

Wurster, P., Maneta, M., Beguería, S., Cobourn, K., Maxwell, B., Silverman, N., et al., 2020. Characterizing the impact of climatic and price anomalies on agrosystems in the northwest United States. Agricult. For. Meteorol. 280, 107778 https://doi.org/10.1016/j.agrformet.2019.107778.

Xiao, G., Liu, W., Xu, Q., Sun, Z., Wang, J., 2005. Effects of temperature increase and elevated CO_2 concentration, with supplemental irrigation, on the yield of rain-fed spring wheat in a semiarid region of China. Agricult. Water Manag. 74 (3), 243–255. https://doi.org/10.1016/j.agwat.2004.11.006.